RESEARCH ARTICLE

Materials and technology of mosaics from the House of Charidemos at Halikarnassos (Bodrum, Turkey)

Kaare Lund Rasmussen[1]* , Thomas Delbey[2], Bjarke Jørgensen[3], Kasper Høegh Jensen[4], Birte Poulsen[5] and Poul Pedersen[6]

Abstract

An excavation in 1856 by Charles T. Newton and a re-excavation in 1990–93 by a joint Danish-Turkish team revealed several mosaic floors in a late-antique *domus* from the fifth century CE, now called the House of Charidemos. Nineteen tesserae from the floor have been analysed by laser ablation inductively coupled plasma mass spectrometry, Raman micro-spectroscopy, scanning electron microscopy with energy dispersive X-ray analysis, and X-ray diffraction. Seven tesserae were made of opaque glass, eleven from various rock/lithic materials, while one of them was a ceramic fragment. This case-study reports the first analyses undertaken of tesserae from late-antique Halikarnassos. The results show the use of recycled Sb–Mn decoloured glass and two types of red glass. A comparison with tesserae from other sites in Anatolia from the same period shows similarities in the base glass composition, but also some particularities of the colouring and opacifying agents used for the mosaic of the House of Charidemos. The characterisation of the stone tesserae shows a homogeneity in the choice of the materials of the same colours, but no certain provenance has been established in the present work mainly due to the lack of comparative materials.

Keywords: Tesserae, Halikarnassos, House of Charidemos, Chemistry, Production methods

*Correspondence: klr@sdu.dkklr

[1] Institute of Physics, Chemistry and Pharmacy, University of Southern
Denmark, Campusvej 55, 5230 Odense M, Denmark
Full list of author information is available at the end of the article

Graphical Abstract

Introduction

Ancient Halikarnassos, modern day Bodrum, is situated on the south-west coast of Asia Minor/Turkey (Fig. 1). The city became famous for the Mausoleum, which was constructed around the mid-fourth century BCE, and was recognised as one of the seven wonders of the ancient world. This period is also recognised as a golden age, which was followed by a period marked by cultural, economic, and political decline. The main reason for this has been attributed to the sack of Halikarnassos by Alexander the Great during his conquest of the East. However, there is now sound archaeological evidence to suggest that the city did indeed have a rise in economic activity during late Antiquity, in fact, the archaeological material seems to suggest another golden age in the history of ancient Halikarnassos [1–7].

In 1856, a series of excavations in Halikarnassos were conducted by the British archaeologist Charles T. Newton. In this period, Newton excavated a building that he called a Roman Villa with floors covered in mosaics. Newton had all the mosaic floors photographed in situ before he had some of them lifted and brought to London. They are now on display in the British Museum.

This 'Roman Villa' was identified again in 1990 and the excavations were revived during a joint Danish-Turkish collaboration from 1990 to 1993 (Fig. 1). These investigations revealed a building with two yards surrounded by more rooms containing a variety of mosaics decorating the floors. Besides the numerous geometrical motifs, many rooms contained mythological figures and scenes such as Dionysos, Europe and the bull, Aphrodite seated in a cockleshell carried by Tritons, Atalante and Meleager, as well as Dido and Aeneas [8]. Room (O), located in the southern part of the building, has a well-preserved mosaic depicting a nymph riding on an ichthyocentaur playing the cithara. The central panel is surrounded by borders with figurative and geometric patterns.

Due to the finding of a Greek dedicatory inscription (found in the mosaic floor of the large apsidal Room F) mentioning the building (*domos*) and the patron, Charidemos, who had financed the luxurious house, it was now named the House of Charidemos [1, 4, 9]. The analysis of the inscription as well as the style and motifs of the mosaic pavements indicate a date of the construction to the mid-fifth century CE [1]. Mosaics during this period were not only an indicator of wealth and prestige but also conveyed the paideia of the owner by including illustrations of ancient Greek myths and episodes from the Greek and Latin epics [1, 4, 8, 10].

The figurative program of the mosaics of the House of Charidemos is certainly exceptional, and the many depictions of the Greek myths as well as those related to the epics of Homer and Vergil may seem surprising during this late period. However, the intensive studies of late Antiquity during the recent decades have illustrated that this is in line with the strong continuity of especially the Greek culture that can also be observed in other media like for instance silver ware and textiles [1–4, 11–13].

Archaeometric studies of late Antique and early Byzantine mosaic tesserae in Anatolia

Several recent publications have shed light on the production and the composition of glass in Anatolia during
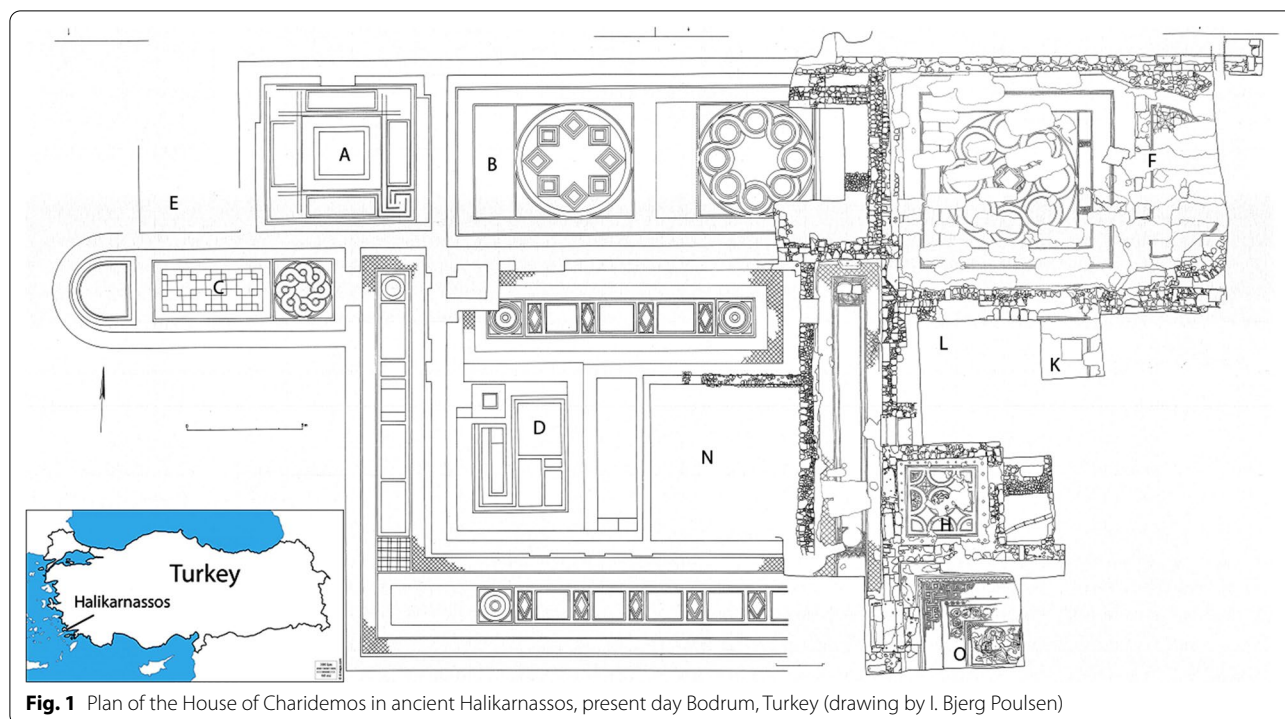
Rasmussen *et al. Heritage Science*   (2022) 10:62

Page 3 of 23

Fig. 1 Plan of the House of Charidemos in ancient Halikarnassos, present day Bodrum, Turkey (drawing by I. Bjerg Poulsen)

the late Roman empire and the early Byzantine period. These publications addressed the questions of the provenance of the raw glass materials, but also the technological evolution occurring in the secondary workshops where the glass was colourised and opacified. Regarding the compositional analysis of glass mosaic tesserae, several studies reported data from single archaeological contexts dated from this transitional period. Most of the sites where mosaic glass samples have been analysed are concentrated in the western and south-western parts of Turkey: Sardis and Aphrodisias [14]; Ephesos [15, 16], Sagalassos [17, 18], and Hierapolis [19]. In the Eastern part, the results of analyses undertaken on glass tesserae from the single site of Tyana were reported by Lachin et al. [20]. In the southern part of Anatolia, glass tesserae from several contexts in Antioch were analysed [21]. Close to the Anatolian coastline, the composition of wall mosaic glass tesserae from several early Christian sites in Cyprus have also been investigated [22].

The question of the techno-chronological evolution of the glass composition has been addressed using glass samples from Pergamon [23, 24]. The results of this diachronic evaluation showed that early Roman period glass can be characterised by the presence of the Sb-decoloured, Mn-decoloured, and mixed Sb–Mn decoloured groups of glass. During the early Byzantine period (fourth–seventh centuries CE), the dominant glass groups were the Levantine I and Levantine II groups

characterised by their high Al and Ca content, and the High-Iron–Manganese–Titanium (HIMT) group, where the raw glass originated from Egypt. Two sub-group of the HIMT glass have also been identified during the early Byzantine period: one with high boron and alumina content (HBAl), and a second one described as "weak HIMT" with higher Ca to Sr ratio correlated to the Mn content.

The publication of the glass tesserae results from the late Roman-early Byzantine site of Kilise Tepe in the south of Turkey included a geographical comparison of the tesserae glass composition with a wide range of data from contemporary sites in Anatolia [25]. The groups of base glass identified were similar to those described at Pergamon (the "weak HIMT" group is referred to as the Foy-2 group). In most of the sites investigated, the tesserae assemblages included both Egyptian (Roman Sb-decoloured, HIMT, and Foy-2) and Levantine (Roman Mn-decoloured and Levantine I) glass. The presence of new colouring and opacifying technologies, different from the ones used in the early Roman times are confirmed at all these sites. Calcium phosphate ($CaPO_3$) and lead–tin (Pb–Sn) compounds were progressively found to substitute the antimonate compounds as opacifying agents, while metallurgical by-products were used to produce brown and red tesserae.

Archaeometric descriptions of stone tesserae including petrographic, mineralogical, and geochemical analyses are quite common in recent archaeological publications

(see e.g., [26–29]). However, few data of stone tesserae from Anatolia have been published to this day. To the best of our knowledge, the study of the tesserae from a sixth century Imperial bath building and a house in Sagalassos is the only archaeometric data of mosaic stones from the late Roman–early Byzantine period in Anatolia [30]. Based on petrographic, mineralogic and isotopic analyses, the results of this study demonstrate the intensive use of white marble from the Dokimeian quarries and green *Cippolino verde* marble from Karystos. Beside these, a wide variety of stones and limestones from different provenances were used. Because of the abundant presence of white and polychrome marble quarries in Turkey and the abundance of archaeological materials, several studies have focused on the description of the geological materials and the provenance of architectural and sculpture fragments from this area [31–39].

Aims of this study

Through archaeometric characterisation of a selection of glass and stone tesserae, the present study aims to provide a first insight about the technology and the materials used for the decoration of the House of Charidemos. By comparing our results of the glass samples from the House of Charidemos to published data from other contemporary sites in Anatolia, the objective is to evaluate how the material from this site support the techno-chronological trend observed in the Anatolian area for the late Roman–early Byzantine periods. The analyses of the stone samples aim at identifying the type of geological materials used and its homogeneity. Comparison with a sample from the quarry of Iasos helps to determine if the material used for the red stone tesserae originate from this place.

Materials and methods
Materials analysed

The mosaic floors of the house of Charidemos are made of tesserae of various colours and materials, including white and polychrome stones, glasses, and ceramics. Generally, the sizes of the tesserae are quite homogeneous, amounting to ca. 8×9 tesserae per dm^2, but smaller tesserae are also present and used for details of for instance faces and hair. Not surprisingly, the smaller tesserae prevail in more detailed parts of the representations like for example the heads of the Seasons of Room F (Fig. 2). A range of colours of stone has been used in all the mosaics. There is a wide range of shades of each colour when considering the observation with the naked eye during fieldwork, wherefore no synoptic colour determination was considered meaningful in the laboratory. White and black/dark blue are by far the most common colour.

Fig. 2 Mosaics from the House of Charidemos. **a** View of the excavation from the south; **b** the floor of Room F; **c** the floor of Room O; season, **d** personification of autumn in Room F; season, **e** personification of summer in Room F (Photos by J. Isager, excavation photos)

A total of 19 tesserae were taken to Denmark for analysis, selected to cover a range of colours. Seven were of glass (purple, red, deep red, and yellow), 11 were stones (grey, white, dark yellow, light red, dark red, and greenish grey) and one was a ceramic (Fig. 3 and Table 1). An additional stone sample from the well-known quarry at Iasos was added (sampled by B. Poulsen).

The tesserae analysed in this study all stem from the mosaic floors in Room F and Room O in the House of Charidemos [40]. Room (F) is a large apsidal room of about $10 \text{ m} \times 14 \text{ m}$ with a mosaic floor damaged by the digging of burials when the site was used as a cemetery during the eighteenth and nineteenth centuries. The apse floor is decorated with geometric patterns that consist of squares with inscribed circles, rosettes, cable-knots, and Maltese crosses. The main room that contained the dedicatory inscription is decorated with geometric and figurative motifs. The dedicatory inscription in front of the apse is flanked by a dog chasing a wild goat, and the central part consists of eight medallions representing
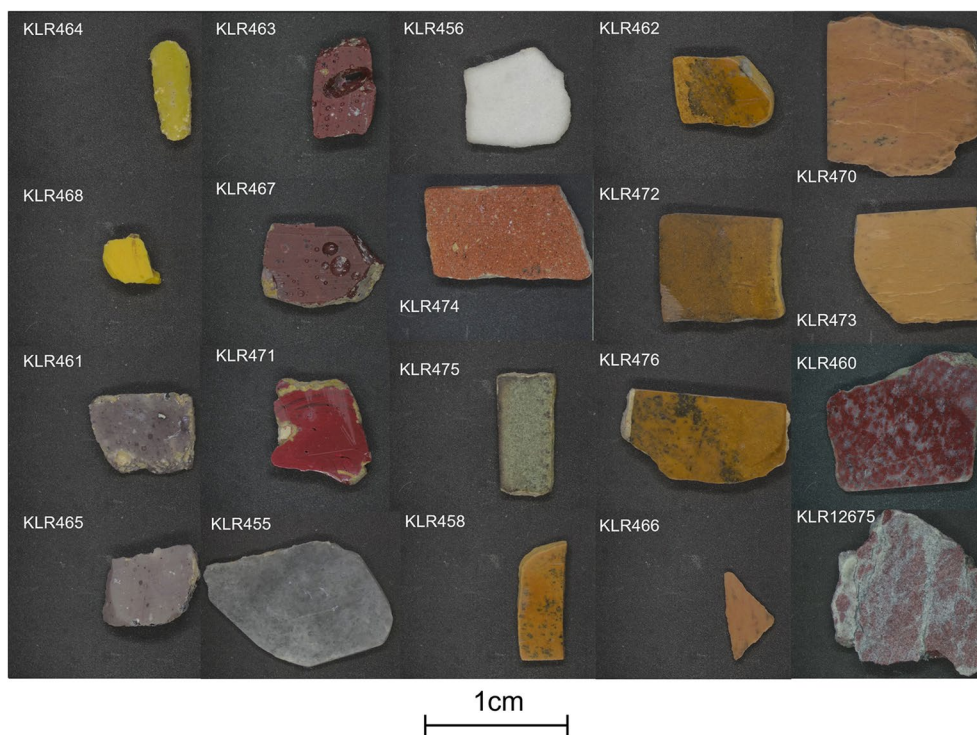
Rasmussen *et al. Heritage Science* (2022) 10:62

Page 5 of 23

Fig. 3 The samples investigated in the present work

animals on a forest background, probably a hunting scene. In the four corner spandrels are winged female seasons characterised by inscriptions.

Methods

Since the analyses had to be non-destructive, all the samples were analysed without preparation for any of the methods applied. However, the tesserae exhibited relatively slick upper surfaces suitable for the analyses. The X-Ray Diffraction (XRD) and µ-Raman Spectroscopy (MRS) measurements have thus been performed on the surface of the samples in a non-destructive way. Most of the stone samples exhibit a slightly weathered top layer on the upper side, and incrusted plaster on the lower side. The analyses have all been performed on the upper side, well knowing that this side has been subjected to some degree of weathering, causing a potential alteration, and consequently some minor minerals can be trapped in the surficial layer, which could also be seen in some of the diffractograms. All 20 samples were analysed with Laser Ablation Inductively Coupled Plasma Mass Spectrometry (LA-ICP-MS) and 18 samples were analysed with XRD and MRS. For the stone samples, the MRS results are not discussed since they provided essentially the same information as the XRD. The SEM–EDS has only been applied on some of the

glass samples in order to elucidate the structure and composition of inclusions.

Scanning electron microscopy with energy dispersive X-ray analysis (SEM–EDS)

The SEM–EDS analysis were performed using a Tescan Vega 3 SEM equipped with an Oxford Instruments microanalysis system and situated at Cranfield Forensic Institute. All the observations were made using the back-scattered electrons (BSE) detector in Univac (variable pressure) mode to enable analysis without coating the specimens. The analysis used an accelerating voltage of 25 kV and a working distance of 15 mm.

µ-Raman spectroscopy (MRS)

The tesserae were analysed using a Thermo Scientific DXR Raman microscope with a 532 nm laser and a $10\times$ objective attached to it and situated at Newtec Engineering A/S. Full-range scan (3500–100 cm^{-1}) was used with a laser power of 10 mW, spectral resolution of 5 cm^{-1} full width half maximum and a spot size of 2.1 µm diameter. The Thermo Scientific DXR Raman microscope is equipped with an Andor CCD camera. The exposure time was between 5 and 15 s with between 5 and 10 stacked exposures depending on the Raman signal of the individual samples (KLR-457: exposure time 15 s, 5

Rasmussen *et al. Heritage Science*   (2022) 10:62

Page 6 of 23

Table 1 Samples included in the present study

Lab No.	Colour	Location	Type	Analysis
KLR461	Purple	Room O	Glass	LA-ICP-MS, XRD, MRS
KLR465	Purple	Room O	Glass	LA-ICP-MS, XRD, MRS
KLR463	Red	Room O	Glass	LA-ICP-MS, XRD, MRS
KLR467	Red	Room O	Glass	LA-ICP-MS, XRD, MRS
KLR471	Deep Red	Room O	Glass	LA-ICP-MS, XRD, MRS
KLR464	Yellow	Room O	Glass	LA-ICP-MS, XRD, MRS
KLR468	Yellow	Room O	Glass	LA-ICP-MS
KLR455	Grey	Room F	Stone	LA-ICP-MS, XRD, MRS
KLR456	White	Room F	Stone	LA-ICP-MS, XRD, MRS
KLR458	Dark Yellow	Room F	Stone	LA-ICP-MS, XRD, MRS
KLR462	Dark Yellow	Room O	Stone	LA-ICP-MS, XRD, MRS
KLR472	Dark Yellow	Room O	Stone	LA-ICP-MS, XRD, MRS
KLR476	Dark Yellow	Room O	Stone	LA-ICP-MS, XRD, MRS
KLR466	Light red	Room O	Stone	LA-ICP-MS, XRD, MRS
KLR470	Light red	Room O	Stone	LA-ICP-MS, XRD, MRS
KLR473	Light red	Room O	Stone	LA-ICP-MS, XRD, MRS
KLR460	Red	Room F	Stone	LA-ICP-MS, XRD, MRS
KLR474	Orange-Red ceramic	Room O	Ceramic	LA-ICP-MS, XRD, MRS
KLR475	Green-Grey	Room O	Stone	LA-ICP-MS, XRD, MRS
KLR12675	Dark red	Iasos quarry	Stone	LA-ICP-MS

The columns encompass: laboratory number, the colour, the find position, the type of tessera, and the analysis undertaken in this study

exposures; KLR-459: 15 s, 8 exposures; KLR-468: 15 s, 5 exposures; KLR-469: 10 s, 8 exposures; KLR-12675: 5 s, 10 exposures). The Spectragryph software was used to process the Raman spectra.

X-ray diffraction (XRD)

The analysis was performed using a PANalytical X'Pert PRO MPD system (PW3050/60) diffractometer with Cu Kα radiation as the source ($\lambda = 1.54$ Å) and a PIXcel3D detector at University of Southern Denmark. The X-ray generator was set to an acceleration voltage of 45 kV and a filament emission current of 40 mA. All

measurements were performed with a 2Θ angle step size of 0.013° and a counting time of 1500 s per step in a range from 5° to 90° 2Θ. Data were collected using a X'Pert Data Collector. The qualitative analysis was performed using Highscore Plus software and Crystal Impact Match software linked to the ICDD PDF-2 database. The analysis of the surface of the samples constituted an important limiting factor. Indeed, the capabilities of detection are lower compared to a classic powder diffraction analysis.

Laser ablation-inductively coupled plasma mass spectrometry (LA-ICP-MS)

The analyses were carried out with an Agilent 8900 triple quadrupole ICP-MS coupled with a ESI New Wave Research NWR 193 ArF excimer laser. The ICP-MS was operated with a plasma power set at 1380 W, a plasma gas flow of 15 L min^{-1}, and an auxiliary gas flow of 0.90 L min^{-1}. Helium was used as carrier gas (800 mL min^{-1}) in single MS mode with no cell gas. Each spot was ablated during 60 s with a laser fluence of 6 J cm^{-1}, a repetition rate of 15 Hz and a spot diameter of 70 μm. Gas blank was recorded during the 10 s warm-up time and the 5 s washout time. Each sample was analysed in triplicates. The ICP-MS was tuned on the glass SRM NIST612 to achieve high sensitivity and stability (RSD < 5%). The plasma condition was monitored with U/Th ratio (0.9–1.1) and ThO/Th ratio was used to assess a low oxide level (ThO/Th < 0.01). The ICP-MS was setup in full-quant mode for the acquisition of 41 masses. The integration times was set to 0.05 s for most of the isotopes. The integration time was increased to provide a better sensitivity for ^{9}Be and ^{82}Se and reduced for the most abundant major elements in order not to overload the detector. Instrumental drift was corrected by regularly measuring the SRM NIST 612. The first 20 s of ablation were considered as pre-ablation and were not used in the calculation of the concentration. The reference samples Corning B and Corning D were measured to evaluate the accuracy. Quantitative data were obtained using the sum normalization approach with NIST 612 as external standard and SiO$_2$ as the internal standard [41]. The results on the SRMs NIST 612 and Corning glass D (Additional file 1) were comparable to the accepted values [42–44].

Results

The LA-ICP-MS quantitative results of the 41 elements selected for 20 tesserae from the House of Charidemos and the sample from the Iasos quarry are listed in the Table 2.

Table 2 Results of the LA-ICP-MS analysis of the 20 tesserae from House of Charidemos in Halikarnassos

Sample	Colour	Na₂O wt%	MgO wt%	Al₂O₃ wt%	SiO₂ wt%	P₂O₅ wt%	SO₃ wt%	K₂O wt%	CaO wt%	TiO₂ wt%	MnO wt%	Fe₂O₃ wt%	CuO wt%	Sb₂O₅ wt%	PbO wt%
KLR461	Purple	16.3	0.633	2.34	67.8	0.104	0.718	0.653	7.04	0.079	2.04	0.523	0.005	1.54	0.020
KLR465	Purple	18.5	0.540	2.12	66.4	0.076	1.16	0.646	6.09	0.076	1.72	0.495	0.026	1.90	0.022
KLR463	Red	16.5	0.899	2.37	62.8	0.231	0.402	1.03	7.24	0.110	0.679	5.10	0.447	0.774	1.23
KLR467	Red	15.8	0.940	2.30	63.4	0.262	0.364	1.01	6.77	0.106	0.396	4.24	0.543	0.728	2.92
KLR471	Deep Red	12.7	1.26	2.88	50.2	0.344	0.270	1.09	6.59	0.267	0.181	2.47	1.87	0.074	18.2
KLR464	Yellow	14.0	0.867	1.99	59.0	0.191	0.641	0.838	5.85	0.089	0.284	1.03	0.032	1.30	13.7
KLR468	Yellow	14.1	0.541	2.25	60.5	0.101	0.448	0.633	6.20	0.090	0.823	0.906	0.015	1.48	11.7
KLR455	Grey	0.004	1.94	0.003	0.053	0.010	0.156	0.001	97.7	0.000	0.001	0.062	0.483	0.010	0.096
KLR456	White	0.002	40.2	0.003	0.056	0.053	0.037	0.000	59.6	0.012	0.001	0.010	0.681	0.087	0.498
KLR458	Dark Yellow	0.013	0.472	1.10	1.90	0.187	0.065	0.070	91.0	0.051	0.091	4.92	30.1	9.18	17.2
KLR462	Dark Yellow	0.017	0.838	1.20	2.14	0.172	0.103	0.110	89.6	0.049	0.121	5.54	37.4	17.0	23.6
KLR472	Dark Yellow	0.021	0.322	0.758	1.31	0.111	0.049	0.075	92.9	0.033	0.164	4.19	18.8	4.52	57.1
KLR476	Dark Yellow	0.023	0.512	1.00	1.58	0.132	0.056	0.114	92.6	0.050	0.053	3.77	19.1	3.59	2.92
KLR466	Light Red	0.015	1.019	2.21	7.38	0.065	0.046	0.722	87.0	0.111	0.125	1.11	15.5	0.413	7.69
KLR470	Light Red	0.019	1.11	3.65	8.95	0.180	0.067	1.048	83.2	0.175	0.105	1.32	17.4	0.310	8.52
KLR473	Light Red	0.012	0.989	2.24	6.63	0.032	0.029	0.744	87.9	0.101	0.125	1.05	14.0	0.201	7.35
KLR460	Red	0.205	0.919	1.86	5.37	0.014	0.011	0.557	89.4	0.068	0.235	1.18	0.990	0.204	12.4
KLR474	Orange-Red ceramic	0.207	1.06	9.12	76.0	0.108	0.082	1.061	8.04	0.479	0.023	3.74	14.7	0.475	32.3
KLR475	Green-Grey	4.14	1.97	11.0	34.3	0.385	0.064	1.750	39.1	0.395	0.675	5.81	18.2	0.866	34.0
KLR12675	Dark-red lasos quarry	0.039	1.11	0.776	1.57	0.059	0.029	0.255	93.2	0.079	0.496	2.24	2.04	0.381	27.1

Sample	Colour	Li µg g⁻¹	Be µg g⁻¹	B µg g⁻¹	V µg g⁻¹	Cr µg g⁻¹	Co µg g⁻¹	Ni µg g⁻¹	Zn µg g⁻¹	Ga µg g⁻¹	Ge µg g⁻¹	As µg g⁻¹	Se µg g⁻¹	Rb µg g⁻¹	Sr µg g⁻¹
KLR461	Purple	4.90	0.309	160	38.1	12.3	9.90	12.9	30.1	2.61	0.675	32.5	1.981	7.78	559
KLR465	Purple	5.26	0.277	180	39.4	14.2	10.6	11.3	47.4	2.37	0.728	41.8	0.377	9.20	471
KLR463	Red	9.48	0.344	163	23.1	15.2	24.1	31.9	105	2.89	0.716	47.8	0.690	11.2	454
KLR467	Red	7.82	0.310	167	17.8	14.3	18.5	25.6	233	2.75	0.681	42.4	0.639	10.5	412
KLR471	Deep Red	4.72	0.397	116	25.1	23.2	210	309	1045	5.48	4.232	921	0.388	6.27	502
KLR464	Yellow	4.57	0.310	149	12.7	10.8	3.22	6.71	52.8	2.16	0.544	73.8	1.973	7.67	377
KLR468	Yellow	4.43	0.290	132	30.9	16.8	5.34	8.04	29.2	2.95	0.671	78.6	4.876	8.76	441
KLR455	Grey	0.17	0.007	0.527	5.68	6.75	0.046	0.647	1.67	0.005	0.008	0.352	0.355	0.019	229
KLR456	White	0.74	0.015	0.388	1.19	6.04	0.037	1.61	3.73	0.008	0.034	0.332	0.550	0.006	136
KLR458	Dark Yellow	4.28	1.04	17.3	130	110	23.2	170	63.1	4.12	0.257	171	0.581	4.90	68.5

Table 2 (continued)

Sample	Colour	Li µg g⁻¹	Be µg g⁻¹	B µg g⁻¹	V µg g⁻¹	Cr µg g⁻¹	Co µg g⁻¹	Ni µg g⁻¹	Zn µg g⁻¹	Ga µg g⁻¹	Ge µg g⁻¹	As µg g⁻¹	Se µg g⁻¹	Rb µg g⁻¹	Sr µg g⁻¹
KLR462	Dark Yellow	2.07	1.10	3.73	218	64.2	7.17	46.0	69.0	3.71	0.230	299	0.603	8.10	132
KLR472	Dark Yellow	1.35	0.795	3.12	154	20.0	37.0	31.1	30.4	2.25	0.201	233	0.540	5.78	42.8
KLR476	Dark Yellow	2.29	0.819	3.40	107	68.4	7.20	42.0	52.4	2.67	0.160	163	0.677	7.62	87.9
KLR466	Light Red	9.98	0.507	20.8	18.5	19.6	3.24	22.1	45.4	3.05	0.594	9.53	0.844	26.5	497
KLR470	Light Red	16.7	0.667	29.0	23.7	29.1	3.63	25.1	49.2	4.30	0.776	9.96	0.736	39.3	478
KLR473	Light Red	10.1	0.504	17.8	20.0	21.4	3.13	20.0	47.1	2.98	0.549	6.49	0.504	27.6	504
KLR460	Red	7.51	0.429	7.62	12.0	16.4	9.58	14.7	24.7	2.36	0.444	1.36	0.490	17.3	1470
KLR474	Orange-Red ceramic	28.4	1.43	27.8	74.4	62.5	8.77	20.0	66.0	12.2	1.46	8.35	0.802	45.2	175
KLR475	Green-Grey	16.1	7.71	9.25	66.4	9.33	10.6	7.80	84.5	16.4	1.21	38.9	0.534	94.3	1516
KLR12675	Dark-red lasos quarry	3.45	0.223	6.45	11.9	11.1	22.8	13.4	65.0	1.16	0.519	2.84	1.11	7.40	958

Sample	Colour	Y µg g⁻¹	Zr µg g⁻¹	Nb µg g⁻¹	Mo µg g⁻¹	Ag µg g⁻¹	Sn µg g⁻¹	Cs µg g⁻¹	Ba µg g⁻¹	La µg g⁻¹	Ce µg g⁻¹	Au µg g⁻¹	Th µg g⁻¹	U µg g⁻¹
KLR461	Purple	6.11	39.2	1.51	6.04	0.416	5.38	0.168	633	6.05	10.9	0.025	0.929	1.04
KLR465	Purple	5.58	38.5	1.47	4.51	0.882	8.36	0.229	399	5.71	10.0	0.063	0.922	0.957
KLR463	Red	5.98	50.8	2.16	2.58	2.80	375	0.461	262	6.44	12.0	0.149	1.32	1.11
KLR467	Red	5.79	49.5	2.13	1.53	3.56	461	0.523	230	6.24	11.9	0.087	1.30	1.06
KLR471	Deep Red	7.31	84.3	3.81	2.20	4.16	9171	0.121	148	7.24	14.6	0.006	1.53	0.828
KLR464	Yellow	4.82	46.8	1.93	1.13	12.2	412	0.310	186	5.27	9.91	0.083	1.25	0.889
KLR468	Yellow	5.37	37.1	1.56	2.05	14.9	349	0.527	308	5.64	10.1	0.155	1.08	1.00
KLR455	Grey	0.119	0.380	0.004	0.081	0.005	0.022	0.001	1.50	0.041	0.068	0.000	0.010	0.815
KLR456	White	0.222	0.552	0.176	0.001	0.002	0.060	0.003	1.11	0.116	0.230	0.000	0.016	0.208
KLR458	Dark Yellow	4.98	22.0	1.61	0.955	0.026	0.233	1.22	55.3	4.19	4.13	0.001	0.744	1.971
KLR462	Dark Yellow	3.62	15.6	1.52	1.83	0.027	0.266	2.15	51.5	3.47	5.33	0.000	0.870	0.736
KLR472	Dark Yellow	5.75	11.2	1.34	1.39	0.012	0.157	1.35	85.4	3.73	5.48	0.003	0.547	0.481
KLR476	Dark Yellow	11.5	14.4	1.70	0.845	0.033	0.303	2.01	30.7	3.19	3.67	0.001	0.787	0.610
KLR466	Light Red	28.1	18.8	1.85	0.152	0.007	0.424	1.69	500	24.2	16.5	0.001	1.86	0.441
KLR470	Light Red	31.2	35.6	3.13	0.159	0.013	0.666	2.21	627	26.6	18.9	0.000	2.88	0.516
KLR473	Light Red	30.0	12.4	1.74	0.126	0.007	0.405	1.66	510	28.3	19.6	0.001	1.92	0.356
KLR460	Red	15.1	18.9	1.39	0.212	0.192	0.400	0.837	98.2	16.0	20.6	0.001	2.86	0.322
KLR474	Orange-Red ceramic	10.3	80.2	11.8	0.516	0.077	1.62	2.70	197	23.5	50.2	0.001	5.89	1.43
KLR475	Green-Grey	14.3	205	18.9	0.527	0.055	3.68	10.4	491	146	210	0.002	24.5	12.5
KLR12675	Dark-red lasos quarry	21.1	27.8	1.60	0.154	0.029	12.1	0.335	44.7	9.64	13.9	0.000	1.67	0.470

The elements are listed in percentage of oxide and are normalized to 100%. The main constituents are listed in weight percent of oxides (wt%) and the minor elements are reported in µg g⁻¹

Rasmussen *et al. Heritage Science*   (2022) 10:62

Page 9 of 23

The glass tesserae

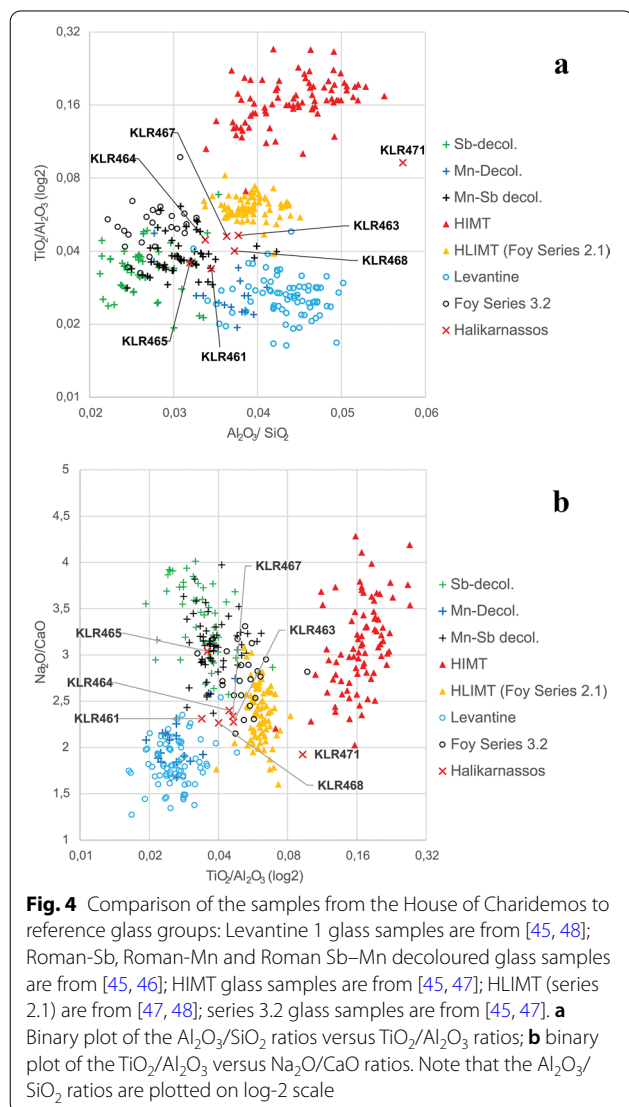#### *LA-ICP-MS bulk analysis results of the base glass*

The seven glass samples from the House of Charidemos show a composition quite typical of the late Antiquity soda-lime-silica glass. The SiO_2 values range from 50 to 67 wt%, Na_2O between 12.0 and 18.5 wt%, and low amounts of K_2O and MgO (both < 1.5 wt%), which is usually considered to indicate the use of natron flux rather than plant ash [45].
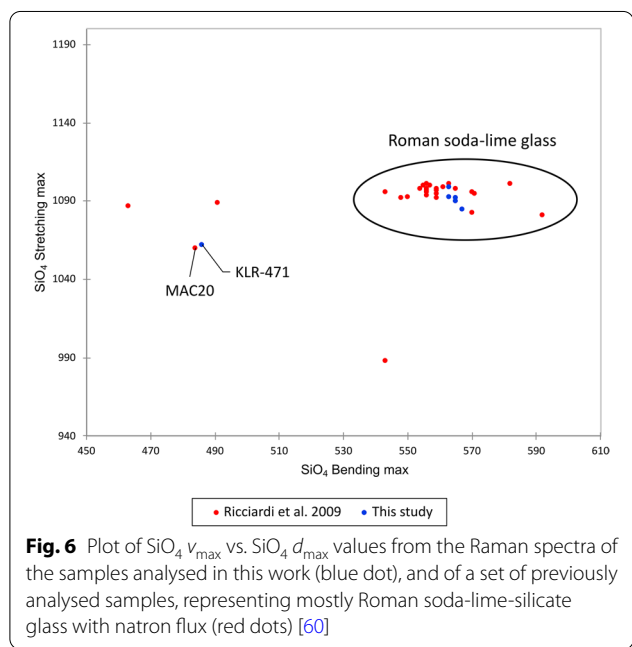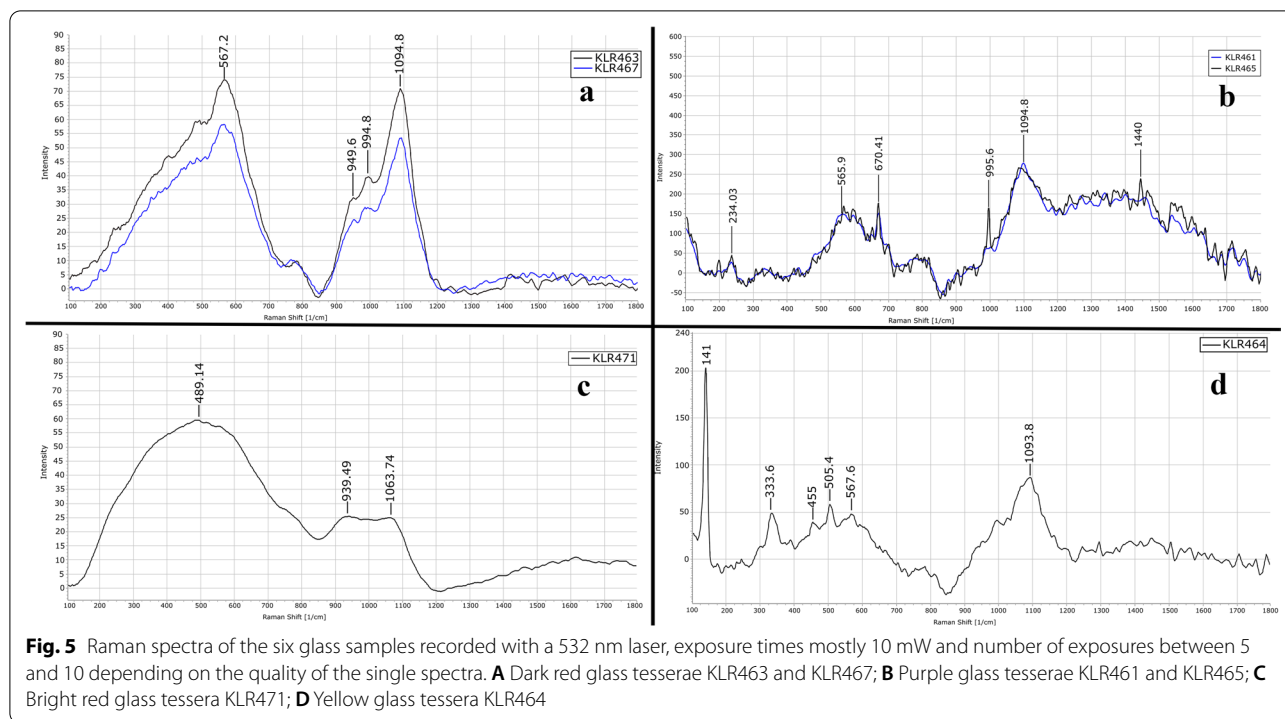
To determine the type of base glass used for these tesserae, our data are compared to a reference dataset which includes samples of the main types of base glass from late antique archaeological contexts [45–48]. The plots shown in Fig. 4 displays a division between the glass groups based on parameters reflecting the mineralogy of the raw materials used in the primary glass workshops. In Fig. 4a, the SiO_2, Al_2O_3, and TiO_2

Fig. 4 Comparison of the samples from the House of Charidemos to reference glass groups: Levantine 1 glass samples are from [45, 48]; Roman-Sb, Roman-Mn and Roman Sb–Mn decoloured glass samples are from [45, 46]; HIMT glass samples are from [45, 47]; HLIMT (series 2.1) are from [47, 48]; series 3.2 glass samples are from [45, 47]. **a** Binary plot of the Al_2O_3/SiO_2 ratios versus TiO_2/Al_2O_3 ratios; **b** binary plot of the TiO_2/Al_2O_3 versus Na_2O/CaO ratios. Note that the Al_2O_3/SiO_2 ratios are plotted on log-2 scale

contents represents the quartz, feldspar, phyllosilicates, and the heavy minerals present in the sand source. The partition between Roman Sb-decoloured glass, series 3.2, HLIMT (series 2.1) and HIMT glass groups on one side, and the Roman Mn-decoloured and Levantine 1 glass groups on the other side, seems to separate the glass made with Egyptian sand and Levantine sand, respectively [49]. The Roman Sb–Mn decoloured glass group, which is seen between these two clusters is pointing to a mixture between the Roman glass decoloured with Sb and Mn [46, 49–51]. An alternative hypothesis could be a mixing of Sb-decoloured glass with HIMT glass containing Mn [46]. On Fig. 4b, the CaO/Na_2O ratio introduces elements related to the carbonate content of the sand and the type of fluxing agent used. The pattern is somehow similar to the one observed in Fig. 4a, showing a clear division between the Roman Mn-decoloured glass, overlapping the Levantine 1 group, and the Roman Sb-decoloured, closer to the HLIMT and series 3.2. groups. The Roman Sb–Mn decoloured samples are located between the two Roman decoloured groups, supporting the hypothesis of a mix.

On the two plots, six of the seven tesserae from the House of Charidemos are located between the Mn-decoloured and the Sb-decoloured glass even if they are not always perfectly overlapping the Sb–Mn decoloured glass from the reference dataset. In Fig. 4a they are quite tightly gathered close to the Sb–Mn decoloured glass reference samples. The red samples KLR463 and KLR467, and the yellow sample KLR468 are slightly shifted toward the HLIMT group, exhibiting higher Al_2O_3/SiO_2 ratios. In Fig. 4b the purple tessera KLR465 is located among the Sb–Mn decoloured glass samples, but the other five samples from Halikarnassos are shifted down with lower values of the Na_2O/CaO ratio. If the data are reduced on the non-chromophore elements, the K_2O and MgO contents of the samples KLR461, KLR465, and KLR464 are in the range of the Sb–Mn decoloured samples whereas the samples KLR463, KLR467, and KLR468 have higher contents (K_2O > 1%, MgO > 0.9%). The deep red tessera KLR471 is an outlier not matching any of the reference groups in the two plots. The composition of this sample is characterised by concentrations of CaO, K_2O, MgO, Al_2O_3, TiO_2, and P_2O_5 higher than in the other six samples. This tessera also shows high amounts of PbO, CuO, and Fe_2O_3, related, or partly related, to the addition of colouring agents as will be explained below.

Considering the seven samples from the House of Charidemos, a correlation is observed between K_2O, MgO, and P_2O_5. This could suggest the presence of fuel ashes in the melt in the secondary workshops when the glass was recycled and/or coloured [18, 52, 53].

Fig. 5 Raman spectra of the six glass samples recorded with a 532 nm laser, exposure times mostly 10 mW and number of exposures between 5 and 10 depending on the quality of the single spectra. **A** Dark red glass tesserae KLR463 and KLR467; **B** Purple glass tesserae KLR461 and KLR465; **C** Bright red glass tessera KLR471; **D** Yellow glass tessera KLR464

Fig. 6 Plot of SiO_4 v_{max} vs. SiO_4 d_{max} values from the Raman spectra of the samples analysed in this work (blue dot), and of a set of previously analysed samples, representing mostly Roman soda-lime-silicate glass with natron flux (red dots) [60]

Raman analysis of the base glass

The Raman spectra of six of the glass tesserae are shown in Fig. 5. Five of the six glass tesserae exhibit the peaks usually attributed to the soda-lime-silica glass type. This identification is made possible by recording the position of the silicon tetrahedron peaks $\delta_{s\ max}$ and $v_{s\ max}$ in

the two envelopes (see e.g., [19, 54, 55]). In Fig. 6 the data from this study are compared to the measurements recorded on Roman soda-lime-silicate glass dated from the first to the fourth century CE by Ricciardi et al. [56]. Most of the samples are tightly gathered with values for $v_{s\ max}$ SiO_4 between 1083 and 1100 cm^{-1} and values for $\delta_{s\ max}$ SiO_4 between 550 and 570 cm^{-1}. Since the dataset from Ricciardi et al. included coloured and colourless glass, it seems that the chromophore ions are not disturbing the silicate network signal. The peaks displayed near 950 cm^{-1} and 990 cm^{-1} in most of the glass tesserae from the House of Charidemos are common in antique soda lime silica glass: the intensity of the first one is related to the amount of alkali metals nanocrystals in the glass network [57, 58]. The second peak located here at 994 cm^{-1} is attributed to the main v_1 mode of Na-sulphate (Na_2SO_4) according to the values published by Mabrouk et al. [59]. However, another interpretation of this band is related to the formation of Ca-rich nanocrystals precipitating in a Ca-saturated glass matrix [56, 57]. The position of the SiO_4 stretching and bending envelopes of these 5 samples from the House of Charidemos are matching in type with the family 3 "$Na_2O + K_2O + CaO$" glass identified by Colomban et al. [60]. In Fig. 6, the proximity between sample MAC20 from Ricciardi et al. and KLR471 is interesting. Sample MAC20 is described as a red tessera altered in green, made of Pb–Na silicate glass, characterised by high CuO (~9 wt%) and PbO

Rasmussen *et al. Heritage Science*   (2022) 10:62

Page 11 of 23

(~ 30 wt%) concentration values, and the presence of degradation products such as Pb-carbonate and Cu-oxides [56]. The remaining red colour in the sample KLR471 could be related to a lower concentration of Cu, or the absence of heavy alteration which would have resulted in a pale green colour provoked by the oxidation of Cu into Cu^{2+}. Moreover, the position of the SiO_4 stretching and bending envelopes for the sample KLR471 is also matching with the family 5 "PbO + NaO" glass according to the classification suggested by Colomban et al. [60].

Pigments and opacifiers

Opaque red glass The three red tesserae KLR463, KLR467, and KLR471 exhibited high quantities of CuO, Fe_2O_3, and PbO. The amount of PbO is much higher in KLR471 (18.2 wt%) and this sample also exhibits higher concentrations of Co, Ni, Zn, Sn, and As. The concentrations of Sb_2O_3 are higher in KLR463 and KLR467 (0.77 wt% and 0.72 wt%, respectively) than for KLR471 (0.07 wt%). The Raman spectra of the samples KLR463 and KLR467 are very similar (Fig. 5A). The main bands are the δ_s SiO_4 band at 1092 cm^{-1} and the ν_s SiO_4 band at 567 cm^{-1}. Their position is relevant for the presence of metallic copper in the glass matrix which is influencing the signal from the SiO_4 network [61]. The Raman spectrum of sample KLR471 is shown in Fig. 5C, and this is different from those of the two previous dark red glass tesserae. The position of two bands related to the

SiO_4 vibrational modes are strongly shifted: the ν_s mode band is broader and shifted between 940 and 1060 cm^{-1}. The δ_s mode band is displayed as a broad band centred around at 500 cm^{-1}. The positions of the symmetric stretching band can be explained by high amounts of Pb in the glass matrix of this sample, which could have been added to ensure the reduction of Cu to its metallic state. The shape and position of the broad symmetric bending band might also originate from degradation of the glass, since Cu^0-rich glass can easily be corroded by acidic water [54]. Even though the direct observation of metallic Cu using Raman spectroscopy is difficult, the results of the XRD analyses on the three opaque red tesserae confirm the presence of metallic copper (Cu^0) in the red tesserae (one of these shown in Fig. 7). The detection of calcite in KLR471 is the only difference seen in the XRD patterns, which could possibly be caused by the presence of secondary calcite from the burial environment.

With the SEM imaging, two types of metal particles are visible in the two red samples KLR463 and KLR467 (Fig. 8). The first type is a ring-shaped particle made of Cu–Sb and Cu–S containing materials. This type of inclusion possibly hints to the presence of metallurgical by-products added to the batch in order to increase the amount of Cu and to provide reducing agents. The second type is a rounded Fe-rich particle which could have been added to ensure the reduction of Cu. A smaller round inclusion ($\approx$ 30 μm diameter, not displayed in
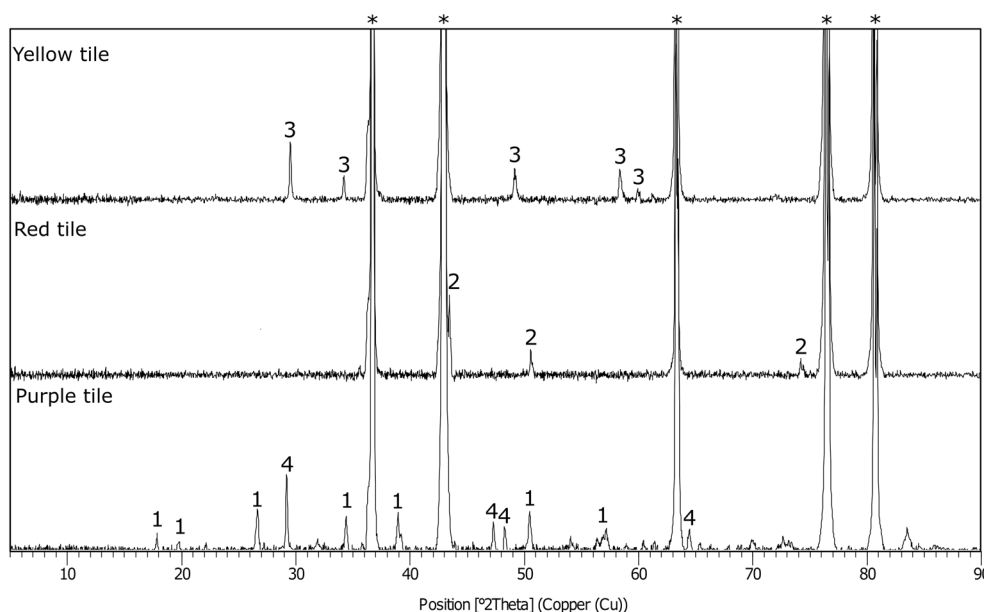

Fig. 7 Diffractograms of three tesserae (KLR463, KLR465, and KLR464) reflecting the mineralogical composition of the purple, red, and yellow tesserae. The background is subtracted. 1 = $CaSb_2O_6$; 2 = Metallic Cu; 3 = $Pb_2Sb_2O_7$; 4 = $CaCO_3$; *peaks from the sample holder. The remainder of the XRD patterns are given in the Additional file 1

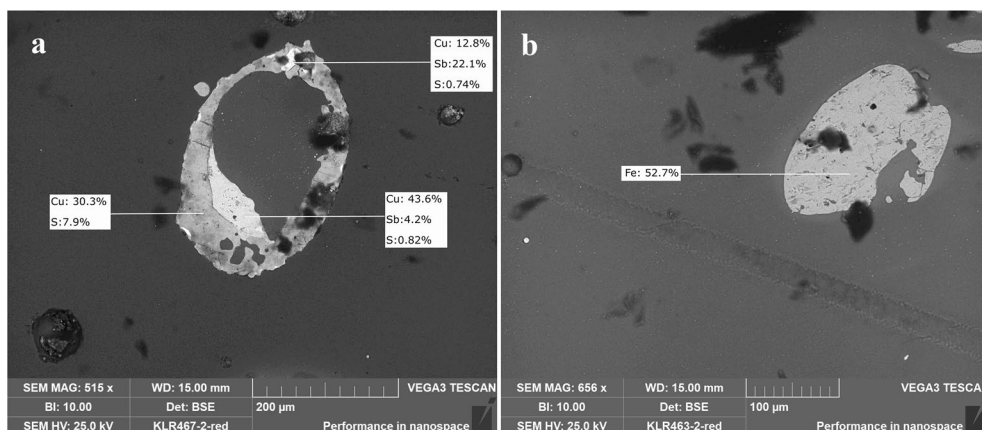Rasmussen *et al. Heritage Science*   (2022) 10:62

Page 12 of 23

Fig. 8 SEM backscattered electron images (BSE) of the dark red samples KLR467 (**a**) and KLR463 (**b**) showing metal Fe, Cu–Sb and Cu–S rich particles
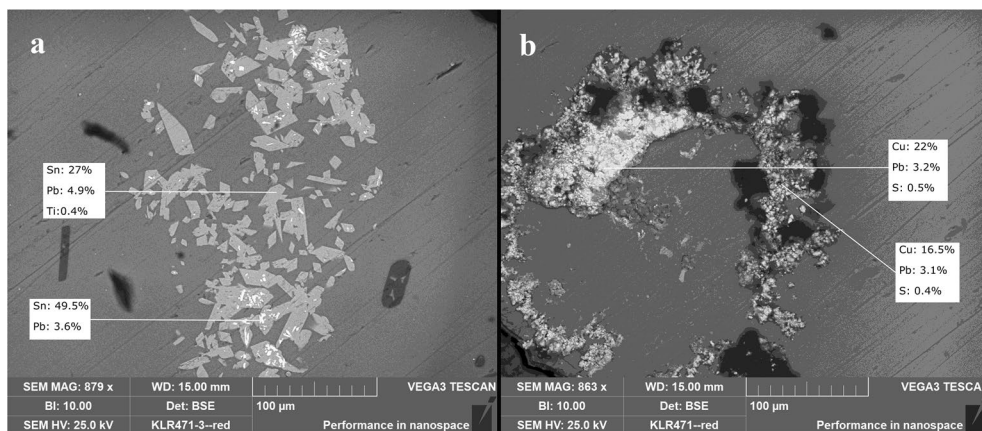

Fig. 9 SEM backscattered electron images (BSE) of the bright red sample KLR471 showing Sn oxide inclusions (**a**), and a likely altered Cu-rich metal inclusion (**b**)

Fig. 8) was analysed in sample KLR463, which showed a composition with high Cu (17.7 wt%), S (8.6 wt%), and Zn (6.8 wt%).

In the red sample KLR471, the SEM–EDS results (Fig. 9) show the presence of tin embedded in larger angular inclusions which reacted with the surrounding glass. In the same sample, a large ring-shaped inclusion similar to the one observed in KLR467 is present. However, the metal particles exhibit a grainy texture and the elemental compositions show higher concentrations of Cu.

Opaque purple glass   The elemental composition of the two purple tesserae KLR461 and KLR465 are characterised by high contents of MnO (2.04 wt% and 1.72 wt%, respectively) and Sb_2O_3 (1.54 wt% and 1.90 wt%, respectively). The Raman spectra of these two samples are very similar (Fig. 5B). The sharp peaks with a medium intensity located at 670 cm^{-1}, the broad peak with a lower intensity at 234 cm^{-1}, and the broad low-intensity peak at 330 cm^{-1} can all be attributed to hexagonal Ca-antimonate ($CaSb_2O_6$) in agreement with the values published by Gedzevičiūtė et al. [62] and Husson et al. [63]. The very low intensity peaks usually located near 520 cm^{-1} is not visible in the present spectra, maybe because of the low crystallinity of the Ca-antimonate, or maybe because it is hidden by the broad bands of the amorphous glass [64]. Sample KLR465 also exhibits a sharp peak at 1440 cm^{-1} which can be assigned to calcite ($CaCO_3$). The main peak of this phase is partially hidden by the broad glass peak, but a blunt shoulder can be seen near 1080 cm^{-1}. The presence of calcite could come from the physical alteration of the tesserae which would have allowed the precipitation of carbonate through water infiltration into fractures in the glass. However,

Rasmussen *et al. Heritage Science* (2022) 10:62

Page 13 of 23

experimental reconstruction of Ca-antimonate opaque glass in laboratory conditions shows that remains of calcite can also be detected if the temperature reached during the melting process was below 1200° [65]. The peak detected at 200 cm^{-1} can be assigned to the orthorhombic phase α-Sb$_2$O$_4$, known as cervantite [66], but this identification is somewhat uncertain. The results of the XRD analyses confirm the presence of CaSb$_2$O$_6$ and CaCO$_3$ in the two purple tesserae. The SEM imaging and the results from the EDS analysis (Fig. 10) show the presence of ≈ 100 μm diameter particles rich in Mn, probably made of decomposed MnO crystals. Sample KLR461 also exhibited a particle of ≈ 40 μm diameter rich in Sb and Ca with low amounts of Mn and S. However, the Mn content detected is likely coming from the Mn-rich particle located nearby.

Opaque yellow glass The yellow glass samples KLR464 and KLR468 showed high values of PbO (13.6 and 11.7 wt%), Ag (12.2 and 14.9 μg g^{-1}), and Sn (412 and 349 μg g^{-1}). The Raman spectrum of sample KLR464 exhibited several peaks attributed to a bindheimite-like mineral (Pb$_2$Sb$_2$O$_7$) located at 141 cm^{-1}, 333 cm^{-1}, 455 cm^{-1}, and 505 cm^{-1} (Fig. 5D). These values are matching the yellow glass tesserae spectrum published by Ricciardi et al. [48] and the RRUF data of bindheimite [67]. Moreover, the XRD diffractogram of KLR464 (Fig. 7) also exhibits the typical pattern of Pb$_2$Sb$_2$O$_7$. This mineral structure has been found in opaque yellow glasses from antiquity [68, 69]. The SEM–EDS results (Fig. 11) showed the presence of scattered and packed Pb–Sb rich particles confirming the identification of bindheimite. With SEM
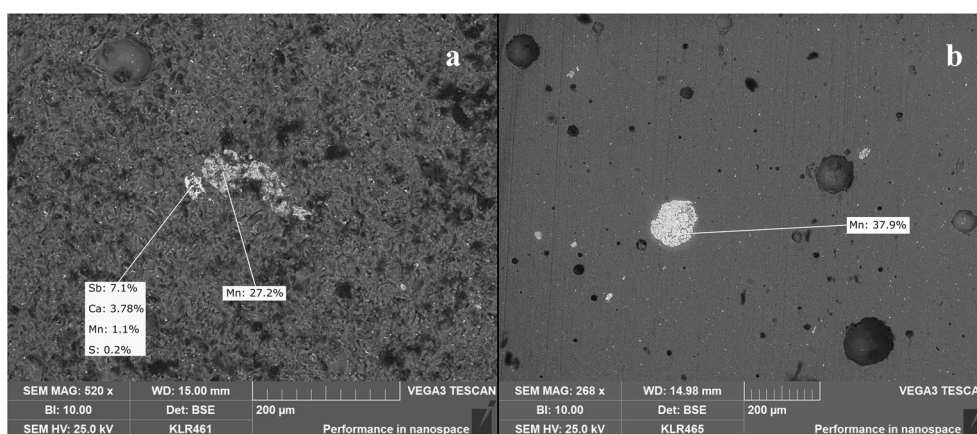

Fig. 10 SEM backscattered electron images (BSE) of the purple samples KLR461 (**a**) and KLR465 (**b**). Both samples show Mn-rich particles and Ca–Sb rich crystals with traces of S
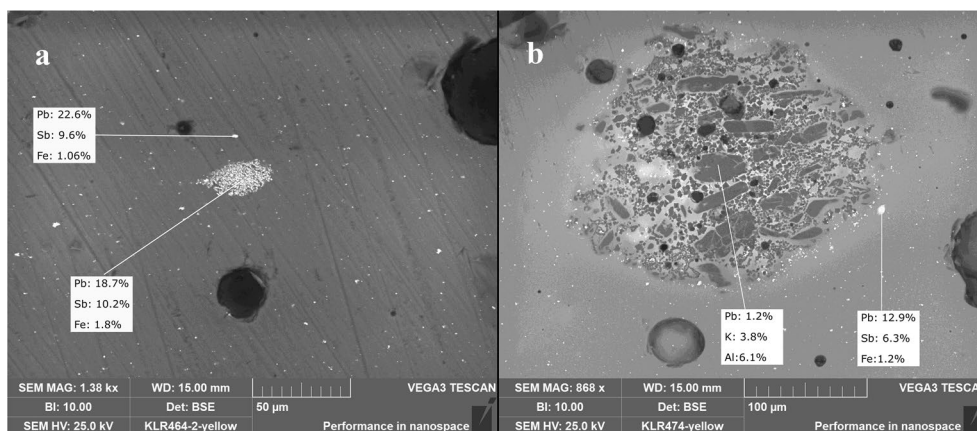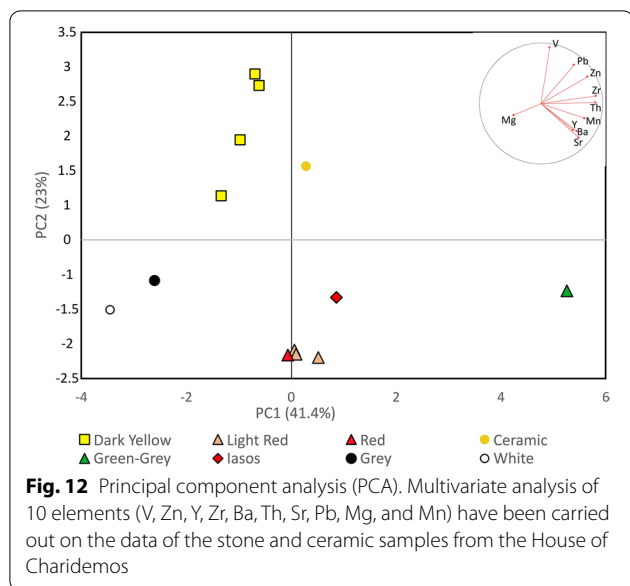

Fig. 11 SEM backscattered electron images (BSE) of the yellow samples; **a** KLR464; **b** KLR474. Both images show the presence of Pb–Sb rich particles

Rasmussen *et al. Heritage Science*   (2022) 10:62

Page 14 of 23

Fig. 12 Principal component analysis (PCA). Multivariate analysis of 10 elements (V, Zn, Y, Zr, Ba, Th, Sr, Pb, Mg, and Mn) have been carried out on the data of the stone and ceramic samples from the House of Charidemos

imaging, the presence of a nodule made of impurities (probably clay) was also detected in this sample.

Stone and ceramic tesserae
Chemical composition

The results of the chemical analysis match the colours of the stone samples and highlight the presence of two groups: the light red and the dark yellow stones. The dark yellow samples KLR458, KLR462, KLR472, and KLR476 are calcareous stones with a CaO-content between 89 and 93 wt% and SiO_2 values between 1.2 and 2.1 wt%.

The composition of this group is quite homogeneous for the major oxides, except for MgO and MnO, with a relative standard deviation RSD > 30%. Compared to the light red samples, the dark yellow tesserae have higher concentration values for Fe_2O_3, Co, Ni, Cu, Cr, Sb, and Pb. The light red samples KLR466, KLR470, and KLR473 are calcareous stones with a CaO-content between 83 and 88 wt%, and SiO_2 values between 6.6 and 8.9 wt%. This group has a quite homogeneous composition but high relative standard deviations (> 30%) for Al_2O_3, P_2O_5, and TiO_2. Compared to the dark yellow samples, they have also higher amounts of Ba, Rb, and Sr. The composition of the dark red tessera KLR460, is somewhat similar, but this sample exhibits higher values of Na_2O, MnO, Ag, and Sr.

The two light-coloured samples have very typical compositions: the grey sample KLR455 is an almost pure CaO (97.7 wt%), with low amounts of MgO (1.9 wt%) and SiO_2 (0.05 wt%), while the white sample KLR456 is a calcareous stone rich in MgO (40 wt%) and CaO (59.6 wt%), and it has also very low concentrations of other major elements. The two samples KLR474 and KLR475 have very different chemical signatures. The ceramic sample KLR474 shows concentration values which could be expected for a calcium rich ceramic matrix with high concentrations of SiO_2, Al_2O_3, and CaO. Sample KLR475 is a calcium rich rock fragments with 39 wt% CaO, 34 wt% SiO_2, and 10.9 wt% Al_2O_3 and high concentration of Ba (491 µg g^{-1}) and Sr (1526 µg g^{-1}).

The dark red reference sample KLR12675 from the quarry in Iasos is a calcareous stone with 93.1 wt% of CaO. The major element composition is quite similar to

Table 3 Results of the XRD analysis on the 13 stone and ceramic samples

Sample	Colour	Cal	Dol	Qz	Ms	Chl	Pl	Kfs	Hem	Gth	Mag	Ti–Fe Spl	Al–Mg Spl	Rt	Di	Crs
KLR455	Grey	+++	o	++	o	o	+	o	o	o	o	o	o	+	+	o
KLR456	White	+++	+++	+	o	o	o	o	o	o	+	o	+	o	o	o
KLR458	Dark Yellow	+++	o	++	o	o	o	o	o	++	o	o	o	o	o	o
KLR462	Dark Yellow	+++	o	+	o	o	o	o	o	++	o	o	o	o	o	o
KLR472	Dark Yellow	+++	o	o	o	o	o	o	o	+	o	o	o	o	o	o
KLR476	Dark Yellow	+++	o	+	o	o	o	o	o	+	o	o	o	o	o	o
KLR466	Light red	+++	o	++	o	o	o	o	o	o	o	+	o	o	o	o
KLR470	Light red	+++	o	++	+	o	o	o	o	o	o	+	o	o	o	o
KLR473	Light red	+++	o	++	o	o	o	o	o	o	o	+	o	o	o	o
KLR460	Red	+++	o	++	++	+	+	o	+	o	o	o	o	o	o	o
KLR474	Orange-Red ceramic	+++	o	+++	o	o	++	+	+	o	o	o	o	+	o	+
KLR475	Green-Grey	+++	o	++	o	o	+++	++	o	o	o	o	o	o	o	o

Mineral abbreviations are reported according to Whitney and Evans [113]: *Cal* calcite, *Dol* dolomite, *Qz* quartz, *Ms* muscovite, *Chl* Chlorite, *Pl* Plagioclase, *Kfs* K-feldspars, *Hem* hematite, *Gth* goethite, *Mag* magnetite, *Spl* spinel, *Rt* Rutile, *Di* Diopside, *Crs* cristobalite

The diffractograms are available in Additional file 1

+++: very abundant, ++: abundant, +: rare, o: absent

Rasmussen *et al. Heritage Science*   (2022) 10:62

Page 15 of 23

the light red and red samples, with lower Al_2O_3, SiO_2, and K_2O. The trace element Ba is much lower than in the red tesserae while the Sn concentrations are higher. The Sr concentration lies between the light red samples and the red one.

A Principal Component Analysis (PCA) was processed on the 12 stone and ceramic samples using ten elements (V, Zn, Y, Zr, Ba, Th, Sr, Pb, Mg, and Mn) as suggested by Poretti et al. [35] and measured by LA-ICP-MS. The PCA was performed with the XLstat software version 2022 1.1. (Addinsoft) on the raw data converted to µg g⁻¹. The PCA analysis showed a pattern similar to the samples of the same colour (Fig. 12). The group of the light red and red stone samples are quite tightly packed at the bottom of the PC1-PC2 plot of Fig. 12 together with the unique reference sample from the Iasos quarry. The dark yellow samples are grouped at the top of the plot, but they show some scattering on the PC2-axis, reflecting a higher compositional variability. The white and grey samples are both located at the bottom left corner of the plot with negative coordinates of both PC1 and PC2. This position results from the low values of major and trace elements other than CaO and MgO. As expected, the ceramic sample and the unknown green-grey stone are separated from the other samples.

Mineralogical composition
The XRD results (Table 3) of the light red tesserae KLR466, KLR470, and KLR473 show a high amount of calcite, the presence of quartz, and traces of Ti–Fe Spinel in all three samples. Traces of muscovite are also identified in the sample KLR470. Even though the intensities of the peaks vary between the samples, the overall mineralogical composition is similar and is in agreement with the elemental results. The diffractogram of the dark red tessera KLR460 is somewhat different from the three light red ones. Calcite, quartz, and muscovite were identified, but chlorite, plagioclase, and hematite were also detected. The presence of hematite could explain the more vivid red colour of this sample.

The results of the XRD analyses of the four dark yellow tesserae KLR458, KLR462, KLR472, and KLR476 were quite similar. The only three phases identified were calcite, quartz, and goethite. However, the intensities of the peaks belonging to goethite are quite different. The main [211] peak has a relatively high intensity in samples KLR458 and KLR462, while it is barely visible in the patterns of samples KLR472 and KLR476. The presence of iron oxyhydroxide is compatible with the yellow colour of these samples and the higher amount of Fe detected by LA-ICP-MS. Goethite could also act as an effective sorbent for As and its presence could therefore explain the higher amount of As detected in the four samples.

The two samples KLR455 and KLR456 show very different diffractograms. The first is mainly comprised of calcite with traces of quartz, plagioclase, rutile, and diopside. The second tessera is a dolomitic stone rich in dolomite and calcite, with traces of Al–Mg spinel and magnetite.

Sample KLR474 is a ceramic sample characterised by a high quantity of quartz and calcite. The presence of cristobalite suggests a high firing temperature [70]. There is also a lower amount of plagioclase, hematite, rutile, and K-feldspar. However, the calcite detected in this sample could also originate from a secondary recrystallisation which could have occurred after the firing of the ceramic.

Discussion
Base glass composition
The binary plots displayed in Fig. 4 show that recycled glass was probably used for six of the seven the glass tesserae of the House of Charidemos analysed in this study. The data shown are consistent with the use of a Sb–Mn decoloured glass for the purple, yellow, and the two red tesserae KLR463 and KLR467. The amount of antimony cannot be used as a marker in the purple and the yellow tesserae because of the presence of Sb-based opacifying/colouring compounds, but the concentration of Sb_2O_5 (> 0.7 wt%) in the two red samples KLR463 and KLR467 is supporting this hypothesis. Similarly, the presence of MnO (> 0.39 wt%) in the two yellow and red samples coloured with lead antimonate and metallic copper, respectively, could also point to the use of this type of base glass. The slight shifts of the Halikarnassos samples observed in Fig. 4 compared to the Sb–Mn decoloured reference glass samples could be caused by the addition of the colouring compounds identified and the presence of fuel ashes in the batch during the mixing/colouring process in the secondary workshops. Indeed, experimental melts made in wood-fired furnaces have revealed that high amounts of K, Mg, Ca, and P can be found in the residues of ashes, which can possibly contaminate the glass melt [52]. The impact of these ashes on the elemental composition of the glass has been observed in the coloured tesserae of Sagalassos [18]. In the samples from the House of Charidemos, the same type of correlation is observed between P_2O_5, K_2O, and MgO. The degree of contamination assessed by the P_2O_5 content seems to roughly correspond to the values measured in Sagalassos for the red and yellow colour groups.

The production of Sb–Mn decoloured glass, identified as the results of recycling and mixing Mn-decoloured and Sb-decoloured glass together [71, 72], has notably been explained by the high price of fresh raw glass chunks and the rarity of this material far from the production centres or the main Roman commercial trade routes. Moreover,

Rasmussen *et al. Heritage Science*   (2022) 10:62

Page 16 of 23

the production and use of glass is known to have suffered a severe decline after the withdrawal of the Roman legions [72]. In the six tesserae Sb–Mn decoloured glass tesserae from Halikarnassos, the distributions of several elements reflecting the sand source composition such as TiO_2, Zr, Nb, Mo, and La are very similar for each "pair" of coloured samples. The deep red sample KLR471 seems to have a composition different from the two other red samples. The higher value for the TiO_2/SiO_2 ratio (0.005) and for the Zr concentration (84 µg g^{-1}) could hint at the use of a different type of base glass. Red glass samples with roughly similar composition has been found in the Apollo Klarios Temple in Sagalassos and has been described as a likely product of early Byzantine glass industry [18].

Comparison with late Antique mosaic tesserae from Anatolia and Cyprus

The composition of the seven glass samples from the House of Charidemos have been compared to the data of mosaic tesserae from contemporary sites located in Anatolia and on Cyprus with a Principal Component Analysis (PCA). Values of the major and minor oxides were processed using the additive log-ratio transformation (ALR) in order to comply with the relative nature of the data and to deal with the closure effect [73, 74]. Silicon oxide (SiO_2) was chosen as the common denominator. Because some of the colouring and opacifying agents identified contain Fe_2O_3, MnO, CuO, PbO, and Sb_2O_3, these elements have been discarded, while Na_2O, MgO, Al_2O_3, SiO_2, K_2O, CaO, and TiO_2 were kept in the analysis. A varimax rotation was applied to maximize the sum of the variance of the squared loadings. The aim was to make stronger associations between the factors and the most meaningful variables in order to achieve a better interpretation of the results [75]. The Rotated PCA (RPCA) was performed using Xlstat software 2022 1.1 (Addinsoft).

The tesserae selected for the comparison were coming from Sagalassos, Antioch, and Cyprus. The samples from Sagalassos have been analysed with Electron Probe Microanalysis (EPMA) and LA-ICP-MS and published by Schibille et al. [18]. The set comprises 48 glass tesserae discovered during the excavation campaigns of the Sagalassos Archaeological Research project, and the site is located about 280 km east of Bodrum. A first group of 28 tesserae originated from the Temple of Apollo Klarios where the mosaics can likely be dated to the first half of the sixth century CE. The second group of 20 tesserae excavated in a Roman bath complex, was dated to the late fourth or early fifth centuries CE. The samples from Antioch have been analysed with SEM–EDS and WDS and published by Wypyski and Becker [21]. Among them,

52 samples were coming from mosaics discovered in the third century CE House of the Drinking Contest and are curated at the Princeton University Art Museum. The second set included 43 samples coming from a mosaic discovered in the Tomb of a Women's Funerary Banquet dated to the middle to late fourth century CE. The samples from Cyprus have been analysed with SEM–EDS and published by Bonnerot et al. [22]. This sample set included 77 glass tesserae from wall mosaics collected in five early Christian sites dated between the fifth and seventh centuries CE.

On the RPC1-RPC2 plot (Fig. 13) a majority of the samples from Cyprus are forming a large, separated cluster at the top of the plot with positive RPC2 coordinates. This position in the plot reflects a higher content of CaO and Al_2O_3, and lower values of Na_2O. On the left side of the plot is seen a tight group which includes most of the tesserae from House of the Drinking Contest in Antioch mainly characterised by lower proportions of K_2O, MgO, and TiO_2. The samples from the Roman Bath and the Apollo Klarios Temple at Sagalassos and the tesserae from the Tomb of a Women's Funerary Banquet at Antioch are forming a wide and looser cluster in the lower half of the plot. Even though these three groups cannot be separated from each other in this plot, the samples from the Roman Bath seem to scatter less in both factorial parameters. Inside the said area, the heterogeneity is mainly coming from the variation of MgO, TiO_2, and K_2O reflected by the RPC1. Six of the seven samples from the House of Charidemos are located inside this dense area with negative RPC2 coordinates. Their compositions
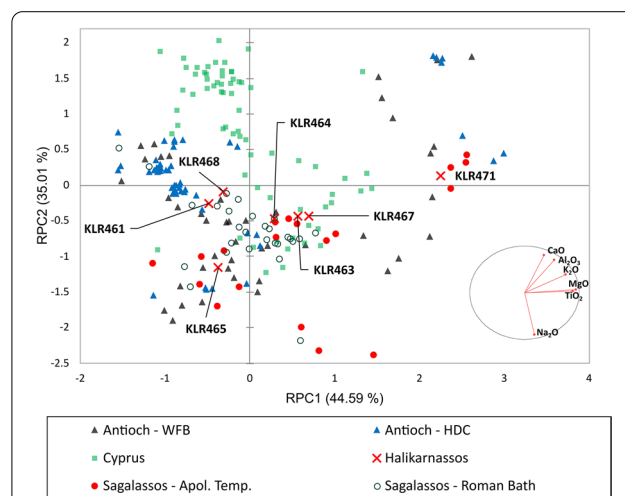
Fig. 13 Principal Component analysis (PCA). Multivariate analysis of seven oxides (Na_2O, MgO, Al_2O_3, SiO_2, K_2O, CaO, and TiO_2) using the compositions of the samples from the House of Charidemos, Antioch [21], Cyprus [22], and Sagalassos [18]

Rasmussen *et al. Heritage Science*   (2022) 10:62

Page 17 of 23

are closest to the tesserae from Sagalassos and the Women's Funerary Banquet at Antioch. Almost all samples gathered on the right side of the PCA plot with RPC1 coordinates above 2, including the sample KLR471 from Halikarnassos, are red and orange samples originating from all the archaeological contexts considered in this comparison, with the Roman Bath at Sagalassos as the only exception.

As already mentioned by Schibille et al. [18], the higher homogeneity of the assemblages from the earlier contexts, such as the House of the Drinking Contest and the Ramon Bath, is striking. The scattering of the seven samples from the House of Charidemos in Fig. 13 seems in line with the dispersion observed for the tesserae from the sites of the Tomb of a Women's Funerary Banquet in Antioch and the Apollos Klarios temple in Sagalassos.

Identification and comparison on the pigments and opacifiers composition

Opaque red glass
The fabrication of opaque red glass using metallic copper in these periods has been investigated in several archaeometric studies (e.g., [50, 76–78]). Our analyses show that samples KLR463 and KLR467 have a similar composition with high Fe, and moderately high Cu, and Sb. This suggests the use Fe as a reducing agent to reduce and maintain Cu in its metallic state. The Sb identified in these two samples (>0.7 wt%) might also have acted as a reducing agent from the oxidation of Sb_2O_3 to Sb_2O_5.

High concentrations of Zn and Sn in red glasses have often been interpreted as caused by using galena or metallurgical by-products in the glass manufacturing process, and the concentrations measured for these two elements in the three red tesserae are higher than in the purple ones. The use of slags or metal scraps as sources of Cu, Sb, and S in the red glasses in the present investigation seems also attested by the ring-shaped inclusions observed with the SEM (Fig. 8). However, the absence of Sn detected in these features might indicate a different origin. The precise nature of the metal inclusions in KLR463 and KLR467 therefore remains somewhat unclear, but further work would help to elucidate this point. The use of copper-rich metal scraps such as brass or bronze for the colouration of Roman red glass has previously been reported in several works [78–81]. The higher concentration of P_2O_5 in these samples compared to the yellow and purple ones suggest the addition of ash during colouring in the secondary workshop to ensure the reduction of Cu [18].

The higher concentrations of Pb, Zn, Sn, As, and Co, and the low amount of Sb in the red tessera KLR471 suggested the use of Sn as opacifier instead of Sb. This is confirmed by the results of the SEM imaging with the

identification of Sn–Pb inclusions. This finding is not surprising since the use of Sn-based opacifier gradually replaced Sb during late Antiquity [18, 82]. Moreover, Sn can act as a strong reducing agent which will keep Cu in its metallic state. The high proportion of Pb in the glass melt could have facilitated the nucleation and the growth of the metallic Cu inclusions. The opaque red tesserae from Apollo Klarios temple in Sagalassos are showing the same type of composition with more than 1 wt% of Sn. It has been suggested that this Sn could originate from tin-rich waste from metallurgy production [18]. Like the samples KLR463 and KLR467, the higher amount of P_2O_5 is likely related to the presence of ashes.

Opaque purple glass
The purple tesserae are opacified with calcium antimonate and the colour is coming from the high proportion of manganese, which is also detected. The manufacturing process and the properties of glass opacified with calcium antimonate is well known [65, 83–85]. Antimony is usually introduced as stibnite (Sb_2S_3) in the glass batch before it turns into roasted stibnite Sb_2O_3 (Sb^{3+}). During the cooling period of the glass, the oxygen penetrates the batch, and the antimony is eventually oxidized to Sb_2O_5 (Sb^{5+}), which forms the trigonal $CaSb_2O_6$ when bonding with the Ca already present in the batch. Manganese is then used to colour the opacified glass to a purple appearance. The mechanisms leading to the purple colouration of the Roman glass using manganese dioxide has been described by Möncke et al. [86] and Bidegaray et al. [87]. The main idea is to bring the Mn-ions into a trivalent oxidation state, which is characterised by a low-spin d_4 configuration exhibiting Jahn–Teller distortions, which will give a strong purple colour. Manganese can be added to the batch as pyrolusite (MnO_2) and its Mn^{4+} ions are readily reduced to Mn^{2+} because of the reducing atmosphere in the furnace. Our results confirm that the oxidation of Mn to its trivalent oxidation state likely took place due to the presence of Sb and Fe. Even though no Fe containing mineral phases have been detected in the Raman or XRD analysis, the addition of a small amount of hematite (Fe_2O_3) to help the Mn oxidation is possible. The ratio Fe:Mn, close to 0.2 is consistent with the data from the melting experimentation of purple glass reported by Bidegaray et al. [87]. In the Raman spectra, the redox reaction involving Sb can maybe be attested by the detection of α-Sb_2O_4 which could have been produced by further oxidation of Sb_2O_3. Our results support the prevalence of the trigonal $CaSb_2O_6$ over the cubic $Ca_2Sb_2O_7$. Moreover, the presence of residual S associated with the Ca–Sb rich crystals confirm the use of stibnite as the source of antimony. Only three purple tesserae from Cyprus are recorded in the comparison

Rasmussen *et al. Heritage Science*   (2022) 10:62

Page 18 of 23

sites considered in this study. However, the composition of these translucent samples is different from the two purple samples from the House of Charidemos, since they have a MnO-content close to 1 wt% and a very low Sb_2O_3 concentration (0.1 wt%). Indeed, the particularity of the purple sample from Halikarnassos is the combination of Mn as colouring agent and the opacifying calcium antimonate. Such a combination has, however, been identified at other sites, such as the four opaque purple tesserae from the Roman villa of Noheda in Spain dated from the fourth–fifth centuries CE [85].

Opaque yellow glass

The use of lead antimonate in Roman glass has been investigated in several studies and summarized by Molina et al. [69]. The first hypothesis is related to the use of Sb litharge from the cupellation of Ag [88] in which Fe could have been added to stabilise the lead-antimonate and enhance the colour [76]. Because of the high amounts of Zn in New Kingdom Egyptian glasses, an alternative method for the production of lead-antimonate has been suggested. Indeed, since Zn would not have survived the high temperatures reached during the processing of silver ore, a mix of roasted galena (PbS) and stibnite (Sb_2S_3) could have been used to synthetize lead-antimonate [83, 89]. The low amount of Zn in our yellow samples KLR464 and KLR468 could point to the use of litharge or maybe of a mix of low-Zn galena with stibnite. The presence of Fe and Sn could originate from an intentional addition to the batch to increase the stability of the lead-antimonate particles or Fe and Sn could originate from impurities present in some of the raw materials [69]. Lead antimonate and lead stannate are commonly detected in the other archaeological contexts investigated. The presence of lead antimonate confirmed in the tesserae from the House of Charidemos connect these yellow tesserae more to the Roman tradition than to the Byzantine one, where lead stannate is more common [25].

The production of the glass tesserae

The base glass used for the tesserae from the House of Charidemos likely included Sb–Mn decoloured recycled glass. The similarity of the values for the elements related to the sand source in the pairs of tesserae made of Sb–Mn glass questions the existence of a single workshop which could have made the recycling and mixing in order to obtain a single glass colour. The heterogeneous distributions of the chemical elements linked to the colouring/opacifying compounds in the samples of the same colour, questions the organisation of the glasswork after the recycling. Indeed, if the existence of workshops specialized in the production of certain glass colour has already been evoked [21, 85], the present data would point to a production with a quite low standardization of the colouring recipes. However, these observations would need a larger set of samples in order to be supported.

Drawing a bigger picture of the glass production from the tesserae of the House of Charidemos is difficult because of the small number of samples analysed. However, it seems that the base glass and the colouring agents identified are matching with what is already known in Anatolia for the late Roman–early Byzantine period. The use of Sb-bearing compounds reflects the continuity of the Roman tradition, but the presence of the deep red tessera KLR471 opacified with Sn also point at the use of new Byzantine glass recipes. The use of recycled glass at Halikarnassos during the fifth century CE might be related to the limited supply of fresh raw glass materials during the late Roman period [72]. Indeed, the transformation of commercial trade routes resulting from the decline of the central Roman power had consequences for the production and distribution of manufactured goods all over the Empire. The production of glass tesserae being limited by the availability of raw materials and the technology needed, workshops must likely have adapted their technology by recycling and mixing available materials.

Origin of the stone samples

The PCA undertaken on a limited number of elements show a proximity between the red stone samples from the House of Charidemos and our reference sample procured from the Iasos quarry. However, the compositional differences prevent to us from drawing a firm link between these tesserae and *marmor Iassence*, the *marmor carium* also known as *cipollino rosso* [90–92]. This very characteristic stone mainly dark red with oars of light red that was used locally from the Hellenistic period, and which was also widely exported to other sites in the Mediterranean from the Severan period onwards. At least three quarries have been identified to the NE of Iasos ([90, 93]: 412; [92]). It became extremely popular during late Antiquity, and it is referred to in literary sources such as Paul Silentiary (Paulus Silentiarius) II, 605–636 ([90]: Fig. 2; [91]).

If the lack of detailed microscopic and petrographic analysis on the samples KLR455 and KLR456 prevent us to provide a description of the texture of the rocks, their elemental composition could match with the identification of calcite marble and dolomitic stone/marble, respectively. A PCA analysis was conducted in order to compare sample KLR455 to the published marble database from Paros, Prokonnesos, Herakleia/Miletos, and Thasos [38]. The results of the PCA and HAC (Hierarchical Agglomerative Clustering) clustering show a proximity between KLR455 and the marble from Herakleia/

Rasmussen *et al. Heritage Science*   (2022) 10:62

Page 19 of 23

Miletos, but the size of the cluster is very small (PCA and HAC plots available in Additional file 1). The mineralogy and the colour of KLR456 could point at a provenance from the quarries of dolomitic marble from Cape Vathy in Thasos, intensively exploited until the second half of the fifth century CE [94]. These attributions can only be considered as tentative, since petrographic and isotopic analysis would be necessary to assess the provenance of the samples with higher certainty. A more detailed examination of the dark yellow and red calcareous samples would also help to elucidate their provenance, even though the use of coloured local limestone can be suggested.

An investigation of the local sources like the Marmora Phrygiae Project related to Hierapolis [95], and the investigations related to Aphrodisias [96, 97] is unfortunately still missing for Halikarnassos and the peninsula. Of particular interest in relation to the House of Charidemos are the investigations of tesserae from the sixth century church of Küçük Tavşan Adası in Bodrum [98]. The preliminary results seem to indicate that the majority of the tesserae stems from Herakleia and a few from Aphrodisias. Among the tesserae is also a stone similar to the quarry at Iasos (TAV 58/2003 and TAV 59/2003), but according to the authors this could also be a local limestone ([98]: 775, Fig. 9). In the Halikarnassos peninsula, the presence of stones like grey, brown, and green andesite are abundant (though not usually used for mosaics), but a marble quarry has been identified in Bozdağ near Myndos [99]. Furthermore, the bluish-grey limestone is easily accessible in the local environment.

The ancient literary sources do not take great interest in the mosaicists who made the numerous time-consuming mosaics in the ancient world, and their actual working processes can mainly be deduced from the mosaic pavements themselves (for discussion of the artisans and their workshops see [2, 100]). The artisans of a mosaic workshop (*officina*) were itinerant, and they would carry out most of their work in the building in which the mosaic floors were laid. The majority of the preserved mosaics was made on location. A few carefully excavated sites have revealed spills of marble, limestone, and other materials from the cutting of the tesserae such as for instance those found in the villa at Morat-Combette in Schwitzerland ([101]: figs. 2–9). Other such findings are recorded from Pont d'Ancy in France ([102]: no. 81), Nabeul in Tunisia ([103]: 79), Rudstone ([104]: pl. 74.1; [105]: 114, no. 1, pl. 101b), and Badminton Park, Gloucestershire in Roman Britain [100]. The scarcity of such recorded findings may, however, be due to the fact that chips and dumps of tesserae have not been correctly identified or interpreted in the excavations [106].

Studies of other mosaic floors found in Halikarnassos indicate that the same basic visual colours (and stones) were used again and again from the Hellenistic period ([40]: 124–130) through the Imperial period [107] up to late Antiquity [6, 7], although no archaeometric analyses have so far been reported on these.

Further analysis of tesserae used in mosaic pavements and locally occurring stone types may indicate if the stones were taken from quarries in the vicinity. This was the case in the villa at Badminton Park ([100]: 148–150). However, some evidence for the production and recycling of stone tesserae should be mentioned [106]. Two finds in either end of the Mediterranean basin and separated by many centuries of time may throw further light on the reuse and production/storing of tesserae. In a house in Pompei (9.12), clearly being restored after the earthquake in 62 CE, tesserae were piled in a room of the house, and they all showed evidence of former use ([108]: 686–687). In Jordan the excavation in Jerash (Gerasa) of the so-called House of the Tesserae revealed a basin/trough that contained thousands of unused white tesserae ready for use when an earthquake in 749 CE stopped all activities in the city [109]. Other excavations such as that of a late Antiquity villa in Aiano-Torraccia near Chiusi (SI) have provided interesting evidence for recycling of glass tesserae. The villa was lavishly restored during the second half of the fourth century CE and furnished with new floors and walls decorated with glass sectilia. When the villa ceased to exist (second half of the fifth–first half of the sixth century CE) workshops recycling the costly materials like bronze, glass and lead were established in the remains of the villa [110]. Such finds are invaluable in relation to questions related to procedures of production, temporarily storing of tesserae, and recycling. They also indicate that tesserae were usually made close to the place where they were going to be used. However, at least one ship cargo (second half of the fourth–first half of the fifth century CE) excavated at the Scauri harbour at Pantelleria shows that tesserae were sometimes shipped over a longer distance [111, 112]. According to the numerous objects including a considerable number of pottery the ship seems to have come to Pantelleria from the coast of Tunisia.

Conclusions

The characterisation of the glass, stone, and ceramic tesserae from the House of Charidemos in Halikarnassos shows that a diversity of the materials were used for the production of the mosaics in private contexts during the late Roman–early Byzantine period in Anatolia. The comparison of the glass composition with other sites in Anatolia showed similarities in the use of base glass materials. The presence of recycled Sb–Mn

Rasmussen *et al. Heritage Science*   (2022) 10:62

Page 20 of 23

decoloured glass and the use of Ca-antimonate and Pb-antimonate are connecting these tesserae to the late Roman tradition. The use of Sb as an opacifying agent shows that this material was still widely used at this period in Halikarnassos and was not yet fully replaced by Sn-rich compounds as it can be seen in the deep red tessera KLR471. The very tight elemental distributions between the samples of similar colours reflecting the same base glass composition could support a hypothesis of secondary workshops specialised in the production of certain colour of tesserae. However, the compositional heterogeneity of elements linked to the colouring process is raising questions about the organisation of the production after the recycling of the glass.

The re-use of materials, sometimes considered as a characteristic of the late Roman period can be interpreted as a consequence of changes in an economical system less globalised and maybe more turned toward short circuit consumption. The characteristics of the stone materials used in the House of Charidemos do not allow us to assess the provenance of the geological materials used in this context. Further investigations using thin-section petrography and perhaps stable isotope analysis would be beneficial in order to determine the type and the origin of the stone materials used for these samples.

Abbreviations
ALR: Additive log-ratio transformation; BSE: Backscattered electron images; HOC: House of Charidemos; LA-ICP-MS: Laser ablation inductively coupled plasma mass spectrometry; XRD: X-ray diffraction; SEM–EDS: Scanning electron microscopy energy dispersive spectroscopy; EPMA: Electron probe microanalysis; HIMT: High-Iron–Manganese–Titanium; HLIMT: High-Lime–Iron–Manganese–Titanium; PCA: Principal component analysis; HAC: Hierarchical Agglomerative Clustering; WDS: Wavelength dispersive X-ray spectrometer.

Supplementary Information
The online version contains supplementary material available at https://doi.org/10.1186/s40494-022-00697-3.

> **Additional file 1.** Results on Corning Glass D and NIST-612. The rest of the diffractograms. PCA plot (F1,F2) comparing the geochemistry of sample KLR455 to marble samples from Paros, Prokonnesos, Herakleia, Miletos and Thasos. Dendrogram of the HAC classification on the coordinates of the PCA.

Author contributions
Conceived and designed the experiments: KLR and TD. Performed the analyses: TD, BJ, and KHJ. Analysed the data: KLR, TD, BJ, and KHJ. Contributed as experts on late Antiquity and Halikarnassos, history, and Roman trade history as well as fieldwork: BP and PP. Wrote the paper, with comments from other participants: KLR and TD. The paper was approved by all authors. All authors read and approved the final manuscript.

Availability of data and materials
The data used in the present study are available in the tables or in Additional files provided.

Declarations

Ethics approval and consent to participate
There are no special ethical issues involved in this work.

Competing interests
It is declared that we have no competing interests.

Author details
[1]Institute of Physics, Chemistry and Pharmacy, University of Southern Denmark, Campusvej 55, 5230 Odense M, Denmark. [2]Cranfield Forensic Institute, Cranfield University, Defence Academy of the UK, Shrivenham SN6 8LA, UK. [3]Newtec Engineering A/S, Stæremosegaardsvej 18, 5230 Odense M, Denmark. [4]ALK-Abelló, Hørsholm, Denmark. [5]School of Culture and Society–Classical Archaeology, Jens Chr. Skous Vej 5, building 1461, 324, 8000 Aarhus C, Denmark. [6]Department of History, Classical Studies, University of Southern Denmark, Campusvej 55, 5230 Odense M, Denmark.

References
1. Poulsen B. Halicarnassus during the imperial period and late Antiquity. In: Karlsson L, Carlsson S, editors. Labraunda and Karia proceedings of the international symposium commemorating sixty years of Swedish archaeological work in Labraunda. Uppsala: The Royal Swedish Academy of Letters, History and Antiquities, Stockholm; 2011. p. 424–43.
2. Poulsen B. Identifying mosaic workshops in late Antiquity: epigraphic evidence and a case study. In: Kristensen TM, Poulsen B, editors. Ateliers and artisans in Roman art and archaeology. Supplement 92 Portmouth: Journal of Roman Archaeology; 2012. p. 129–44.
3. Poulsen B. Patrons and viewers: reading mosaics in late Antiquity. In: Birk S, Poulsen B, editors. Patrons and viewers in late Antiquity. Aarhus: Aarhus University Press; 2012. p. 167–87.
4. Poulsen B. City personifications in late Antiquity. In: Kristensen TM, Birk S, Poulsen B, editors. Using images in late Antiquity. Oxford: Oxbow Books; 2014. p. 209–26.
5. Poulsen B. A pilgrim flask from Halicarnassus. In: Karlsson L, Carlsson S, Bild Kullberg J, editors. Λαβρυς studies presented to Pontus Hellström. BOREAS. Uppsala studies in ancient Mediterranean and near Eastern civilizations. Uppsala: Uppsala Universitet; 2014. p. 479–95.
6. Poulsen B. The necropolis outside the Myndos Gate in Halikarnassos–monuments and mosaics. In: Mortensen E, Poulsen B, editors. Death and Burial in Karia. Halicarnassian studies. Odense: University Press of Southern Denmark; 2016. p. 11–108.
7. Poulsen B. A mosaic in Halicarnassus: cultural interelations between Halicarnassus and the Dodekanese during late Antiquity. In: Poulsen B, Pedersen P, Lund J, editors. Karia and the Dodekanese cultural interrelations in the Southeast Aegean II early Hellenistic to early Byzantine. Oxford and Philadelphia: Oxbow Books; 2021. p. 285–92.
8. Elder Pt. Naturalis Historia (Book XXVI).
9. Isager S. The late Roman villa in Halicarnassus. The inscription. In: Isager S, Poulsen B, editors. Patron and pavements in late Antiquity. Halicarnassian studies. Odense: Odense University Press; 1997. p. 24–9.
10. Vitruvius. De architectura (Book VII).

11. Leader-Newby RE. Silver and society in late antiquity: functions and meanings of silver plate in the fourth to seventh centuries. London: Routledge; 2017.

12. Leader-Newby R. Personifications and paideia in LATE Antique mosaics from the Greek East. In: Personification in the Greek World. London: Routledge; 2017. p. 231–46.

13. Poulsen B. Consideration on motifs and mosaic workshops: the case of Halikarnassos. In: The proceedings of IV international Mosaic Corpus of Türkiye: the Mosaic Bridge from past to present Bursa. 2008. p. 101–10.

14. Brill RH, Stapleton CP. Chemical analyses of early glasses: volume 3: the years 2000, 2011, reports, and essays; 1999.

15. Uhlir K. Naturwissenschaftliche Untersuchungen an antiken Gläsern aus Ephesos mittels µ-RFA und REM/EDS; 2004.

16. Uhlir K, Melcher M, Schreiner M, Czurda-Ruth B, Krinzinger F. SEM/EDX and m-XRF investigations on ancient glass from Hanghaus 1 in Ephesos/Turkey. In: Drauschke J, Keller D, editors. Glass in Byzantium e production, usage, analyses. Mainz: RGZM; 2010. p. 47–64.

17. Degryse P, Schneider J, Poblome J, Waelkens M, Haack U, Muchez P. A geochemical study of Roman to early Byzantine Glass from Sagalassos, South-west Turkey. J Archaeol Sci. 2005;32(2):287–99.

18. Schibille N, Degryse P, Corremans M, Specht CG. Chemical characterisation of glass mosaic tesserae from sixth-century Sagalassos (south-west Turkey): chronology and production techniques. J Archaeol Sci. 2012;39(5):1480–92.

19. Neri E, Morvan C, Colomban P, Guerra MF, Prigent V. Late Roman and Byzantine mosaic opaque "glass-ceramics" tesserae (5th–9th century). Ceram Int. 2016;42(16):18859–69.

20. Lachin M, Serra C, Silvestri A, Molin G. Vitreous mosaic from Tyana (Cappadocia). Late Antique/early Byzantine Glass in the Eastern Mediterranean Izmir. 2009. p. 171–83.

21. Wypyski MT, Becker L. Glassmaking technology at Antioch: evidence from the Atrium House Triclinium and later mosaics. The arts of Antioch–art historical and scientific approaches to Roman Mosaics Worcester MA. Worcester Art Museum; 2005. p. 115–75.

22. Bonnerot O, Ceglia A, Michaelides D. Technology and materials of early Christian Cypriot wall mosaics. J Archaeol Sci Rep. 2016;7:649–61.

23. Schibille N. Late Byzantine mineral soda high alumina glasses from Asia Minor: a new primary glass production group. PLoS ONE. 2011;6(4): e18970.

24. Rehren T, Connolly P, Schibille N, Schwarzer H. Changes in glass consumption in Pergamon (Turkey) from Hellenistic to late Byzantine and Islamic times. J Archaeol Sci. 2015;55:266–79.

25. Neri E, Jackson M, O'Hea M, Gregory T, Blet-Lemarquand M, Schibille N. Analyses of glass tesserae from Kilise Tepe: new insights into an early Byzantine production technology. J Archaeol Sci Rep. 2017;11:600–12.

26. Barca D, Fiorenza E, D'Andrea M, Le Pera E, Musella M, Sudano F, et al. Chemical and petrographic characterization of stone and glass tesserae in the Nereid and Geometric Mosaics from the S. Aloe Quarter in Vibo Valentia-Calabria, Italy. Minerals. 2019;9(12):729.

27. Veritá M, Lazzarini L, Tesser E, Antonelli F. Villa del Casale (Piazza Armerina, Sicily): stone and glass tesserae in the baths floor mosaics. Archaeol Anthropol Sci. 2019;11(1):373–85.

28. Miletić S, Šmuc A, Dolenec M, Miler M, Mladenović A, Gutman Levstik M, et al. Identification and provenance determination of stone tesserae used in mosaics from Roman Celeia, Slovenia. Archaeometry. 2022. https://doi.org/10.1111/arcm.12742.

29. Gomez-Laserna O, Irto A, Irizar P, Lando G, Bretti C, Martinez-Arkarazo I, et al. Non-invasive approach to investigate the mineralogy and production technology of the Mosaic Tesserae from the Roman Domus of Villa San Pancrazio (Taormina, Italy). Curr Comput Aided Drug Des. 2021;11(11):1423.

30. Corremans M, Degryse P, Wielgosz D, Waelkens M, editors. The import and the use of white marble and coloured stone for wall and floor, revetment at Sagalassos. In: Interdisciplinary studies on ancient stone proceedings of the IX association for the study of marbles and other stones in antiquity (ASMOSIA) Conference, Tarragona; 2009.

31. Matthews K. The establishment of a data base of neutron activation analyses of white marble. Archaeometry. 1997;39(2):321–32.

32. De Paepe P, Moens L, De Donder J. Provenance assignment of archaeological marbles in the museum of Ballıhisar (Central Anatolia, Turkey). Anatolia antiqua Eski Anadolu. 2005;13(1):161–70.

33. Yavuz A, Turk N, Koca M. Geological parameters affecting the marble production in the quarries along the southern flank of the Menderes Massif, SW Turkey. Eng Geol. 2005;80(3–4):214–41.

34. Koralay T, Kılınçarslan S. A multi-analytical approach for determining the origin of the marbles in Temple-A from Laodicea ad Lycum (Denizli-Western Anatolia, Turkey). J Cult Herit. 2016;17:42–52.

35. Poretti G, Brilli M, De Vito C, Conte AM, Borghi A, Günther D, et al. New considerations on trace elements for quarry provenance investigation of ancient white marbles. J Cult Herit. 2017;28:16–26.

36. Prochaska W, Ladstätter S, Ambros G, Mitthof F. Material-specific investigation and marble-provenance analysis of inscription plaques in the sanctuary of Apollo Hylates/Cyprus. Jahreshefte des Österreichischen Archäologischen Institutes in Wien. 2018;2018(86):199–220.

37. Scardozzi G. The provenance of marbles and alabasters used in the monuments of Hierapolis in Phrygia (Turkey): new information from a systematic review and integration of archaeological and archaeometric data. Heritage. 2019;2(1):519–52.

38. Prochaska W, Attanasio D. The challenge of a successful discrimination of ancient marbles (part I): a databank for the marbles from Paros, Prokonnesos, Heraklea/Miletos and Thasos. J Archaeol Sci Rep. 2021;35: 102676.

39. Antonelli F, Nestola F. An innovative approach for provenancing ancient white marbles: the contribution of x-ray diffraction to disentangling the origins of Göktepe and Carrara marbles. Sci Rep. 2021;11(1):1–12.

40. Poulsen B. The new excavations in Halikarnassos. A preliminary report (1990–1991). In: Isager J, editor. Hekatomnid Caria and the Ionian Renaissance. Halicarnassian studies. Odense: Odense University Press; 1994. p. 115–33.

41. Gratuze B, Blet-Lemarquand M, Barrandon J-N. Mass spectrometry with laser sampling: a new tool to characterize archaeological materials. J Radioanal Nucl Chem. 2001;247(3):645–56.

42. Jochum KP, Weis U, Stoll B, Kuzmin D, Yang Q, Raczek I, et al. Determination of reference values for NIST SRM 610–617 glasses following ISO guidelines. Geostand Geoanal Res. 2011;35(4):397–429.

43. Wagner B, Nowak A, Bulska E, Hametner K, Günther D. Critical assessment of the elemental composition of corning archeological reference glasses by LA-ICP-MS. Anal Bioanal Chem. 2012;402(4):1667–77.

44. Vicenzi EP, Eggins S, Logan A, Wysoczanski R. Microbeam characterization of corning archeological reference glasses: new additions to the smithsonian microbeam standard collection. J Res Natl Inst Stand Technol. 2002;107(6):719.

45. Maltoni S, Silvestri A, Marcante A, Molin G. The transition from Roman to late Antique glass: new insights from the Domus of Tito Macro in Aquileia (Italy). J Archaeol Sci. 2016;73:1–16.

46. Foster HE, Jackson CM. The composition of late Romano-British colourless vessel glass: glass production and consumption. J Archaeol Sci. 2010;37(12):3068–80.

47. Foy D, Picon M, Vichy M, Thirion-Merle V. Caractérisation des verres de la fin de l'Antiquité en Méditerranée occidentale: l'émergence de nouveaux courants commerciaux. Échanges et commerce du verre dans le monde antique. 2003. p. 41–85.

48. Ceglia A, Cosyns P, Nys K, Terryn H, Thienpont H, Meulebroeck W. Late antique glass distribution and consumption in Cyprus: a chemical study. J Archaeol Sci. 2015;61:213–22.

49. Schibille N, Sterrett-Krause A, Freestone IC. Glass groups, glass supply and recycling in late Roman Carthage. Archaeol Anthropol Sci. 2017;9(6):1223–41.

50. Silvestri A, Tonietto S, Molin G, Guerriero P. The palaeo-Christian glass mosaic of St. Prosdocimus (Padova, Italy): archaeometric characterisation of tesserae with antimony-or phosphorus-based opacifiers. J Archaeol Sci. 2012;39(7):2177–90.

51. Schibille N. Islamic glass in the making: chronological and geographical dimensions. Leuven: Leuven University Press; 2022.

52. Paynter S. Experiments in the reconstruction of Roman wood-fired glassworking furnaces: waste products and their formation processes. J Glass Stud. 2008;50:271–90.

53. Cottam S, Jackson C. Things that travelled: precious things for special people? 2018.

54. Tournié A, Prinsloo LC, Colomban P. Raman classification of glass beads excavated on Mapungubwe hill and K2, two archaeological sites in South Africa. J Raman Spectrosc. 2012;43(4):532–42.

Rasmussen *et al. Heritage Science*   (2022) 10:62

Page 22 of 23

55. Koleini F, Pikirayi I, Colomban P. Revisiting Baranda: a multi-analytical approach in classifying sixteenth/seventeenth-century glass beads from northern Zimbabwe. Antiquity. 2017;91(357):751–64.

56. Ricciardi P, Colomban P, Tournie A, Macchiarola M, Ayed N. A non-invasive study of Roman Age mosaic glass tesserae by means of Raman spectroscopy. J Archaeol Sci. 2009;36(11):2551–9.

57. Colomban P, Etcheverry MP, Asquier M, Bounichou M, Tournié A. Raman identification of ancient stained glasses and their degree of deterioration. J Raman Spectrosc. 2006;37(5):614–26.

58. Yadav AK, Singh P. A review of the structures of oxide glasses by Raman spectroscopy. RSC Adv. 2015;5(83):67583–609.

59. Ben Mabrouk K, Kauffmann TH, Aroui H, Fontana MD. Raman study of cation effect on sulfate vibration modes in solid state and in aqueous solutions. J Raman Spectrosc. 2013;44(11):1603–8.

60. Colomban P, Tournie A, Bellot-Gurlet L. Raman identification of glassy silicates used in ceramics, glass and jewellery: a tentative differentiation guide. J Raman Spectrosc. 2006;37(8):841–52.

61. Colomban P, Schreiber HD. Raman signature modification induced by copper nanoparticles in silicate glass. J Raman Spectrosc. 2005;36(9):884–90.

62. Gedzevičiūtė V, Welter N, Schüssler U, Weiss C. Chemical composition and colouring agents of Roman mosaic and millefiori glass, studied by electron microprobe analysis and Raman microspectroscopy. Archaeol Anthropol Sci. 2009;1(1):15–29.

63. Husson E, Repelin Y, Vandenborre M. Spectres de vibration et champ de force de l'antimoniate et de l'arseniate de calcium $CaSb_2O_6$ et $CaAs_2O_6$. Spectrochim Acta A. 1984;40(11–12):1017–20.

64. Tuschel D. Why are the Raman spectra of crystalline and amorphous solids different. Spectroscopy. 2017;32(3):26–33.

65. Druenert F, Palamara E, Zacharias N, Wondraczek L, Möncke D. Ancient Roman nano-technology: insight into the manufacture of mosaic tesserae opacified by calcium antimonate. J Eur Ceram Soc. 2018;38(14):4799–805.

66. Cody CA, DiCarlo L, Darlington RK. Vibrational and thermal study of antimony oxides. Inorg Chem. 1979;18(6):1572–6.

67. RUFF, Database of Raman spectroscopy, X-ray diffraction and chemistry of minerals.

68. Galli S, Mastelloni M, Ponterio R, Sabatino G, Triscari M. Raman and scanning electron microscopy and energy-dispersive x-ray techniques for the characterization of colouring and opaquening agents in Roman mosaic glass tesserae. J Raman Spectrosc. 2004;35(8–9):622–7.

69. Molina G, Odin G, Pradell T, Shortland A, Tite M. Production technology and replication of lead antimonate yellow glass from New Kingdom Egypt and the Roman Empire. J Archaeol Sci. 2014;41:171–84.

70. Gliozzo E. Ceramic technology. How to reconstruct the firing process. Archaeol Anthropol Sci. 2020;12(11):1–35.

71. Jackson C, Paynter S. A great big melting pot: exploring patterns of glass supply, consumption and recycling in Roman Coppergate, York. Archaeometry. 2016;58(1):68–95.

72. Freestone IC. The recycling and reuse of Roman glass: analytical approaches. J Glass Stud. 2015;57:29–40.

73. Aitchison J. The statistical analysis of compositional data. J R Stat Soc Ser B (Methodol). 1982;44(2):139–60.

74. Greenacre M. Compositional data analysis in practice. London: Chapman and Hall/CRC; 2018.

75. Reimann C, Filzmoser P, Garrett RG. Factor analysis applied to regional geochemical data: problems and possibilities. Appl Geochem. 2002;17(3):185–206.

76. Freestone I, Stapleton CP. Composition technology and production of coloured glasses from Roman mosaic vessels. Oxbow; 2015.

77. Bandiera M, Lehuédé P, Verità M, Alves L, Biron I, Vilarigues M. Nanotechnology in Roman Opaque Red Glass from the 2nd Century AD. Archaeometric investigation in Red Sectilia from the decoration of the Lucius Verus Villa in Rome. Heritage. 2019;2(3):2597–611.

78. Bandiera M, Verità M, Lehuédé P, Vilarigues M. The technology of copper-based red glass sectilia from the 2nd century AD Lucius Verus villa in Rome. Minerals. 2020;10(10):875.

79. Basso E, Invernizzi C, Malagodi M, La Russa M, Bersani D, Lottici P. Characterization of colorants and opacifiers in roman glass mosaic tesserae through spectroscopic and spectrometric techniques. J Raman Spectrosc. 2014;45(3):238–45.

80. Barca D, Basso E, Bersani D, Galli G, Invernizzi C, La Russa MF, et al. Vitreous tesserae from the calidarium mosaics of the Villa dei Quintili, Rome. Chemical composition and production technology. Microchem J. 2016;124:726–35.

81. Maltoni S, Silvestri A. A mosaic of colors: investigating production technologies of roman glass tesserae from Northeastern Italy. Minerals. 2018;8(6):255.

82. Freestone I, Bimson M, Buckton D, editors. Compositional categories of Byzantine glass tesserae. In: Proceedings of the Annales du 11e Congres de l'Association Internationale pour l'Histoire du Verre, Bale; 1990.

83. Shortland AJ. The use and origin of antimonate colorants in early Egyptian glass. Archaeometry. 2002;44(4):517–30.

84. Lahlil S, Biron I, Cotte M, Susini J. New insight on the in situ crystallization of calcium antimonate opacified glass during the Roman period. Appl Phys A. 2010;100(3):683–92.

85. Schibille N, Boschetti C, Valero Tévar MÁ, Veron E, de Juan AJ. The color palette of the mosaics in the Roman villa of Noheda (Spain). Minerals. 2020;10(3):272.

86. Möncke D, Papageorgiou M, Winterstein-Beckmann A, Zacharias N. Roman glasses coloured by dissolved transition metal ions: redoxreactions, optical spectroscopy and ligand field theory. J Archaeol Sci. 2014;46:23–36.

87. Bidegaray A-I, Godet S, Bogaerts M, Cosyns P, Nys K, Terryn H, et al. To be purple or not to be purple? How different production parameters influence colour and redox in manganese containing glass. J Archaeol Sci Rep. 2019;27: 101975.

88. Mass JL, Wypyski M, Stone R. Malkata and Lisht glassmaking technologies: towards a specific link between second millennium BC. Archaeometry. 2002;44(1):67–82.

89. Shortland A, Nicholson P, Jackson C. Lead isotopic analysis of Eighteenth-Dynasty Egyptian eyepaints and lead antimonate colourants. Archaeometry. 2000;42(1):153–7.

90. Lazzarini L, Cancelliere S, Pierobon Benoit R. Il marmo di Iaso: cave, uso, caratterizzazione e indagini archeometriche. Iasos e la Caria Nuovi studi e ricerche, ed. 2005. p. 2–6.

91. Bruno M. Quarry blocks in marmor Iassense from the Balik Pazari at Iasos (Turkey). In: Gutiérrez AG-M, Mercadal PL, de Llanza IR, editors. Interdisciplinary studies on ancient stone: proceedings of the IX association for the study of marbles and other stones in antiquity (ASMOSIA) Tarragona: Institut Català d'Arqueologia Clàssica (ICAC); 2009. p. 706–14.

92. Berti F, Peirano D. Il marmo iasio e alcuni tra i manufatti a esso collegati. Marmora. 2014;10:45–58.

93. Benoit RP. Il territorio di Iasos: nuove ricerche (2006–2008). In: Karlsson L, Carlsson S, editors. Labraunda and Karia proceedings of the international symposium commemorating sixty years of Swedish archaeological work in Labraunda. Uppsala: The Royal Swedish Academy of Letters, History and Antiquities, Stockholm; 2011. p. 389–424.

94. Al-Bashaireh K. Ancient white marble trade and its provenance determination. J Archaeol Sci Rep. 2021;35: 102777.

95. Ismaelli T, Scardozzi G. Ancient quarries and building sites in Asia Minor. Research on Hierapolis in Phrygia and other cities in southwestern Anatolia: archaeology, archaeometry, conservation, Edipuglia, Bari. 2016.

96. Long L. Regional marble quarries. C Ratté and P de Staebler, Aphrodisias V: The Aphrodisias regional survey, Darmstadt. 2012. p. 165–201.

97. Russell B. Mapping the marble quarries. In: Smith RRR, Lenaghan J, Sokolicek A, Welch K, editors. Aphrodisias papers, 5: excavation and research at Aphrodisias, 2006–2012. Supplement 103. Portsmouth: Journal of Roman Archaeology; 2016. p. 255–67.

98. Pelosi C, Santamaria U. The 6th century A.D. Floor mosaic of the Church of Küçük Tavşan Adası (Bodrum). Characterization of the constitutive materials, finding of the Quarries of origin. In: Şahin M, editor. 11th international colloquium on ancient mosaics. Istanbul; 2011. p. 769–78.

99. Pedersen P, Berkaya B. Bozdag—an ancient town and marble quarry near Myndos on the Halikarnassos Peninsula. Halicarnassian studies. Odense: Odense University Press; 2008. p. 43–51.

100. Wootton W. Mosaic production in 4th-c. Britain: materials, makers and making at Badminton Park. In: Kristensen TM, Poulsen B, editors. Ateliers and artisans in Roman art and archaeology. Supplement 92. Portmouth: Journal of Roman Archaeology; 2012. p. 145–68.

101. Agustoni C. Tesselles et déchets de taille à Morat-Combette (Suisse). In: Paunier D, Schmidt C, editors. La mosaïque gréco-romaine VIII. Lausanne; 2001. p. 480–9.
102. Stern H. Recueil général des mosaïques de la Gaule I.1. Paris; 1957.
103. Darmon J-P. Nympharum domus. Les pavements de la maison des Nymphes à Néapolis (Nabeul, Tunisie) et leur lecture. Leiden; 1980.
104. Donderer M. Die Mosaizisten der Antike und ihre wirtschaftliche und soziale Stellung Erlangen; 1989.
105. Cookson NA. Romano-British mosaics: a reassessment and critique of some notable stylistic affinities. Cambridge: University of Cambridge; 1984.
106. Polidoro L. Scarichi e accumuli di tessere musive. Proposte di linee interpretative. In: Cecalupo C, Erba ME, editors. Atti del XXV Colloquio dell'Associazione Italiana per lo Studio e la conservazione del mosaic. Roma; 2020. p. 637–47.
107. Poulsen B. The mosaics of the Salmakis fountain in Halikarnassos. In: Trovabene G, Bertoni A, editors. XII Colloquio AIEMA. Paris; 2015. p. 367–72.
108. Varone A. Un nuovo pavimento musivo pompeiano in corso di restauro al momento dell'eruzione vesuviana del 79 d.C. In: Guidobaldi GA, Guidobaldi F, editors. Atti del III Colloquio dell'Associazione italiana per lo studio e la conservazione del mosaico. Bordighera; 1996. p. 681–94.
109. Lichtenberger A, Raja R. Mosaicists at work: the organisation of Mosaic production in early Islamic Jerash. Antiquity. 2017;91(358):998–1010.
110. Cavalieri M. La villa tardoantica di Aiano (2005–2011/2014–2018). Bilancio di dodici anni di attività dell'UCLOUVAIN in Val d'Elsa (San Gimignano, SI). Bollettino di Archeologia. 2019(3):159.
111. Abelli L, Baldassari P, Tusa S. Lo scavo subacqueo del Porto di Scauri nell'Isola di Pantelleria. In: Attema A, Nijboer A, Zifferero A, editors. Papers in Italian archaeology, 6 communities and settlements from the Neolithic to the Early Medieval period. Oxford; 2005. p. 403–5.
112. Tusa S. La pietra. In: Tusa S, Zangara S, La Rocca R, editors. Il relitto tardoantico di Scauri a Pantelleria. Palermo; 2009. p. 169–72.
113. Whitney DL, Evans BW. Abbreviations for names of rock-forming minerals. Am Mineral. 2010;95(1):185–7.

Publisher's Note
Springer Nature remains neutral with regard to jurisdictional claims in published maps and institutional affiliations.